A first RM-based search for gas at the periphery of galaxy clusters with POSSUM

Paris Gordon-Hall

A thesis submitted for the degree of
Bachelor of Science (Honours)
The Australian National University

October 2024

Except where otherwise indicated, this thesis is my own original work.
None of this thesis was produced by me prior to the commencement of Honours.
Data was collected by me for the first cross-match. For the second cross-match the data was not yet publicly available so my supervisor collected it. Code for Galactic foreground subtraction was provided by my supervisor. Some assistance was also provided by my supervisor with the creation of the Stokes I overlays, and for calculating the angular distance between each RM and the nearest galaxy cluster.

Paris Gordon-Hall
24 October 2024

To my mum, thank you for your unwavering support in every path I have taken and for being a role model I can always look up to.

Acknowledgments

This thesis would not have been possible without the invaluable support of my supervisor, Dr. Craig Anderson. His insightful contributions and thoughtful feedback have shaped every aspect of this work. Thank you for your guidance, ideas, and coding assistance, as well as for the many productive meetings.

A heartfelt thank you to Sarah Bradbury for being my PhD buddy this year, and for her consistent encouragement, support, and advice.

I am also deeply grateful to Prof. Naomi McClure-Griffiths and the members of the RSAA Radio Astronomy group for their helpful questions, feedback, and encouragement during my updates.

Special thanks to Antoine Marchal for his assistance with obtaining eROSITA X-ray data.

Lastly, I want to express my appreciation to my fellow Honours students, both at RSAA and in other disciplines, for their camaraderie and support throughout this challenging year.

Abstract

This study uses Faraday rotation measure (RM) data from the Polarisation Sky Survey of the Universe's Magnetism (POSSUM) observed with the Australian Square Kilometre Array Pathfinder (ASKAP) to conduct the first systematic search for magnetised gas and shocks in the peripheral regions of galaxy clusters. The regions beyond the virial radius of clusters are believed to contain a large fraction of a cluster's baryonic content. They are also sites where various important astrophysical phenomena occur such as accretion and merger shocks, which are believed to heat the WHIM, accreted gas, and play an important role in structural evolution. Recent research has demonstrated that RMs from ensembles of point-like radio sources located behind the clusters, which are called "RM grids", are able to be used to detect magnetised gas in this region in clusters. Previously it has been difficult to study this region due to the large timescales required by other methods such as X-ray emission, or because existing RM grids were not sufficiently dense. In the mostly unexplored area beyond the virial radii of six massive galaxy clusters, this study undertakes a search for RM enhancements associated with magnetised gas. I selected the clusters such that they were known to host hot gas, weigh at least $10^{14} M_{\odot}$, were already observed by POSSUM, and the cluster infall region occupied at least one square degree of sky area to ensure that sufficient RMs of background sources penetrated the cluster atmosphere. Therefore, given a large number of background sources and RMs, this method opens a new observational window for studying the regions beyond the virial radii of massive galaxy clusters. I find RM structures in the Triangulum Australis cluster, and the Abell 3391 cluster, that are notably unusual compared to typical extragalactic regions. The Triangulum Australis cluster shows an RM grid with a variety of structure, with coherent patches of elevated |RM| values within and beyond the infall region. The Abell 3391 cluster has an extraordinarily large RM value beyond the splashback radius, and another substantial RM value close to the splashback radius. I find that these RM enhancements are statistically significant clustered outliers with evidence for potential diffuse radio emission, and an asymmetric X-ray core which suggests a disturbed cluster undergoing active mergers or accretion. I calculate the estimated magnetic field strengths for the coherent RM features in the Triangulum Australis cluster, with one of the features presenting values on the same order of magnitude as expected for cosmic web filaments. I provisionally conclude that the Triangulum Australis cluster contains magnetised infalling gas from outside the cluster and suggest that the Abell 3391 cluster contains a shock. My results suggest that several tens of such systems will likely be observed by POSSUM, and more in the future with the forthcoming SKA.

Contents

List of Figures

List of Tables

Chapter 1

Introduction

This chapter motivates the study of gas at the periphery of galaxy clusters, and the novel methods we use to probe this gas in this thesis is set out as follows: Section 1.1 introduces the concept of galaxy clusters and the hot gas that suffuses them, and the concept of rotation measure (RM) grids as a new window on this gas. Section 1.2 sets out the key objectives for this thesis, which are broadly (1) to determine whether a sample of nearby clusters show RM enhancements consistent with the presence of magnetised gas beyond the virial radius; (2) whether these signatures might trace gas accretion or shocks. Lastly, section 1.3 provides an outline to the rest of the thesis.

1.1 Scientific Motivation

Clusters of galaxies, which are the largest collapsed objects in the Universe, are filled with hot, ionised, X-ray-emitting plasma. This plasma, known as the intracluster medium (ICM), contains most of the baryonic mass in galaxy clusters. It significantly influences galaxy evolution through processes such as ram-pressure stripping. Additionally, the ICM plays a crucial role in the evolution of the entire cluster, where many of the stars and metals in the Universe are formed [Simionescu et al., 2021]. The ICM also has an important role in determining the clusters' gravitational dynamics and their use in probing cosmological parameters [Simionescu et al., 2021; Bulbul et al., 2024]. Further studies of galaxy clusters, particularly in the more unexplored regions (see below), could help explain tensions between cosmological parameter constraints obtained from the primary cosmic microwave background (CMB) and those obtained from current galaxy cluster studies [Xu et al., 2022]. The gas beyond the virial radii of galaxy clusters has been largely unexplored in research despite these peripheral regions being expected to contain a large fraction of the Universe's hot, diffuse, baryonic matter. X-ray and S-Z techniques have been primarily used for galaxy cluster studies to date and they have largely focused on the centres where gas densities and therefore X-ray emissivity and S-Z effects are the highest. Using these techniques in the outskirts of clusters where gas becomes sparse is highly inefficient and requires long integration times. For example, Simionescu et al. [2021] estimates it would take more than 10 years with current instrumentation to observe the entire gaseous extent of even a single nearby massive galaxy cluster. Therefore new approaches are valuable and the Polarisation Sky Survey of the Universe's Magnetism (POSSUM) RM grids (explained further in Chapter 2) address this problem by utilising Faraday RMs to 'back-illuminate' magnetised gas in these peripheral regions.

This thesis aims to determine whether Faraday RMs measured by the revolutionary POSSUM survey being observed with the Australian Square Kilometre Array Pathfinder (ASKAP) radio telescope (all defined and discussed in Chapter 2) will allow us to probe the extended magnetoionic structure of clusters and their surroundings in greater detail than previously seen [Anderson et al., 2021]. Indeed the RM grids obtained will be "the most comprehensive ever obtained" due to its factor of 30 increase in the areal sky density of polarised background sources and coverage of the southern sky [Gaensler et al., submitted]. With POSSUM we expect to receive 30-50 RMs per square degree [Gaensler et al., submitted].,[Vanderwoude et al., in press], compared to only 1 RM per square degree from the previous state of the art. At the moment we lack detailed information on the extent of the magnetic fields and their relationship with the dynamics of clusters. Magnetic fields' effects on galaxy cluster formation will be able to be explored greater with the polarimetric data from POSSUM, and the increase in the RM measurements in the outskirts of clusters.

1.2 Objectives

In this thesis we aim to undertake a new search for RM enhancements beyond their virial radii of six massive galaxy clusters. These clusters have already been observed and verified by POSSUM, and the cluster infall region occupies at least one square degree of sky area, ensuring the region of interest will be thoroughly probed by the POSSUM RM grid. Our project utilises the novel method of RM grids (they are dense ensembles of RMs measured towards background point-like radio sources) which we hypothesise will allow us to detect magnetised gas, shocks, and accretion flow well outside the virial radii of galaxy clusters.

1.3 Thesis Outline

This thesis has six chapters. Chapter 1 motivates the study of gas at the periphery of galaxy clusters, and states the objectives of this work. Chapter 2 outlines the technical and scientific background as well as previous work in the relevant literature. Chapter 3 explains the experimental design, data quality evaluation, sample selection, and Galactic foreground subtraction. Chapter 4 presents the results and analysis of searching for coherent RM features and outliers as well as broader cluster analysis. Chapter 5 discusses the main results, physically interprets the RM enhancements identified, and presents calculations of the magnetic field strength for features of interest in the Triangulum Australis cluster. Chapter 6 summarises the key results from this work, and proposes future directions for this research.

Chapter 2

Background and Related Work

This chapter outlines the technical background, technical innovations and scientific background in this field as well as previous work in the relevant literature. Section 2.1 explains rotation measures (RM) and RM grids, section 2.2 introduces the POSSUM survey, 2.3 introduces ASKAP, section 2.4 describes progress in X-ray observations, section 2.5 describes the application of RM grids to the study of galaxy clusters, and section 2.6 discusses the significance of the peripheral gas of clusters.

2.1 Rotation Measure and RM Grids

Magnetic fields are astrophysically important in diverse cosmic environments [Beck and Wielebinski, 2013], [Johnston-Hollitt et al., 2015], and one of the most powerful techniques we have for measuring magnetic fields is Faraday rotation of linearly polarised radio sources by intervening magnetised plasma [Gardner and Whiteoak, 1966]. The RM quantifies the amount of Faraday rotation, which encodes information about the line of sight magnetic field strength and direction [Gardner and Whiteoak, 1966]. The Faraday RM is calculated by obtaining measurements at several wavelengths of how the polarisation angle changes. For a background polarised source, the simplest way of finding the RM is when a plot of polarisation angle vs. wavelength-squared results in a linear relationship, with the gradient representing the RM. In a magnetoionised medium, radiation experiences propagation effects and the phase velocity is different depending on whether the polarised light is right-handed or left-handed circularly polarised. Polarisation can be described using Stokes parameters I, Q, U and V. Stokes I represents the total intensity, Q represents the horizontal or vertical linear polarisation, U represents the polarisation along vectors of 45 degrees with respect to Q, and V represents the left-handed or right-handed circular polarisation. The Stokes parameters are defined as:

$$I = \epsilon_x^2 + \epsilon_y^2 = \epsilon_0^2$$

,

$$Q = \epsilon_x^2 - \epsilon_y^2 = \epsilon_0^2 \cos 2\beta \cos 2\chi$$

,

$$U = 2\epsilon_x^2\epsilon_y^2 \cos(\phi_y - \phi_x) = \epsilon_0^2 \cos 2\beta \cos 2\chi$$

,

$$V = 2\epsilon_x^2\epsilon_y^2 \sin(\phi_y - \phi_x) = \epsilon_0^2 \sin 2\beta$$

, where ϵ_0 is the total magnitude of the electric field, and β is the degree of ellipticity. The degree of polarisation is given by

$$\frac{\sqrt{U^2 + Q^2 + V^2}}{I}$$

and the angle of linear polarisation is given by

$$\theta = \frac{1}{2} \arctan \frac{U}{Q}$$

. Faraday rotation happens when

$$\int n_e B \cdot dl \neq 0$$

where $n_e\text{cm}^{-3}$ is the thermal electron density, and B(μ G) is the magnetic field. The amount of Faraday rotation is given by

$$\delta\psi = \phi\lambda^2$$

where ϕ is the Faraday depth, ψ is the polarisation angle, and λ is the observing wavelength. The Faraday depth, which is the amount of Faraday rotation per λ^2 as a function of distance along the line of sight, is given by

$$\phi = 0.812 \int_{source}^{telescope} n_e \mathbf{B} \text{ds rad m}^{-2}$$

.

A RM grid is a collection of Faraday RMs, which can be plotted together on a region of the sky [Vanderwoude et al., in press]. We measure RMs towards ensembles of radio sources lying beyond clusters to form an RM grid.

2.2 Polarisation Sky Survey of the Universe's Magnetism (POSSUM) as a Revolutionary New RM Grid Experiment

POSSUM is a new radio polarisation sky survey that is a successor of NVSS (NRAO VLA Sky Survey) [Gaensler et al., submitted]. POSSUM will conduct a sensitive 1 GHz radio polarisation survey covering 20 000 square degrees of the Southern sky with ASKAP. The POSSUM Collaboration produces RM (Rotation Measure) catalogues using the POSSUM data reduction and processing pipeline [Vanderwoude et al., in press]. Using this they construct RM grids. Once they have done this, they assess data quality, RM grid densities, and typical RM uncertainties in each band and their dependence on frequency, bandwidth, and Galactic latitude. Before collecting polarisation parameters, they also separate foreground diffuse emission from the polarisation spectra of the background components. The data from POSSUM will allow us to probe the extended magneto-ionic structure of galaxy clusters and its surroundings in extraordinary detail [Anderson et al., 2021].

2.3 Australian Square Kilometre Array Pathfinder (ASKAP)

ASKAP's unique survey capabilities are something that POSSUM will exploit in order to improve our understanding of magnetic fields in diverse cosmic environments, including but not limited to galaxy clusters and the overall cosmic web and intergalactic medium (IGM) [Gaensler et al., submitted].

ASKAP has a phased array feed and this gives it an instantaneous field of view that covers 31 deg^2 at 800 MHz [Hotan et al., 2021]. It has a two-dimensional array of 36x12 m antennas with baselines ranging from 22 m to 6 km, and 10 arcsec resolution imaging. ASKAP is also able to create images of large sky areas efficiently with its 288 MHz instantaneous bandwidth and a third axis of rotation on each antenna, which gives ASKAP excellent polarisation performance. Its frequency range is between 700 - 1800 MHz and has already been used in surveys attempting to improve our understanding of many aspects of the radio Universe [Hotan et al., 2021]. These features allow ASKAP to observe a large area of sky quickly, meaning that it is possible to obtain a dense RM grid over the entire visible sky, which has previously been impossible.

ASKAP is a radio interferometric array that observes the sky for POSSUM, which is now $\approx 20\%$ complete. ASKAP is located in a radio-quiet zone which is important for the usually occupied 800-900 MHz range in the main survey band of POSSUM. The only possibility for interference is during rare atmospheric ducting events, however, the data is automatically flagged and therefore has a negligible impact on POSSUM's data quality [Gaensler et al., submitted]. The ASKAP observatory maintains and operates the POSSUM-specific pipeline which does interferometric calibrating and imaging, producing images, data cubes, and other products. The bandpass is derived from observations of the unpolarised calibrator source PKS B1934-638 [Gaensler et al., submitted].

2.4 X-Ray Observations as a Tracer of the Cluster ICM

Surveys in the X-ray have been the main means of studying hot gas in galaxy clusters to date, and they have mostly explored the central regions. Athena is scheduled for launch in the early 2030s as the first systematic study of the Warm-Hot Intergalactic

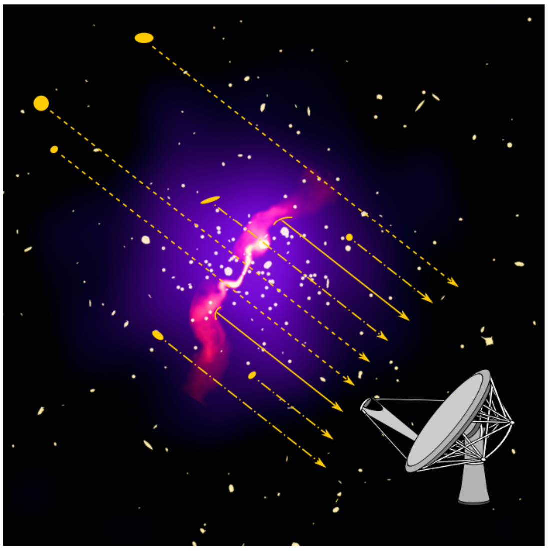

Figure 2.1: Schematic diagram of an RM grid experiment for a nearby galaxy cluster from Johnston-Hollitt et al. [2015]. Lines indicate different path lengths to polarised sources.

Medium (WHIM) [Simionescu et al., 2021]. Previous X-ray telescopes have explored properties of the ICM and have spent lots of exposure time observing in cluster outskirts such as Suzaku, Chandra, and Planck. These observations allowed a glimpse at the hottest and densest large-scale structures that connect massive galaxy clusters to the cosmic web, and they have detected an inhomogeneous gas density. There is clumping that becomes more apparent at the virial radius in simulations, however X-ray observations are not yet able to map the gas further out or routinely probe structures in the infall region of clusters [Simionescu et al., 2021]. The virial radius is approximately R_{200} which encloses a density contrast of $200\times$ the critical density of the Universe. This is often used as the boundary of galaxy clusters [Su et al., 2019]. The infall region is defined as the region between the virial radius and the splashback radius.

2.5 RM Grids as a New Window on the Outskirts of Galaxy Clusters

RM grids can be used to study magnetic fields in many environments, including but not limited to galaxy clusters. Figure 2.1 shows a schematic diagram of the concept of an RM grid experiment.

The first example of a large area survey where a large RM grid was formed was NVSS, and they provided important information on the geometry and direction of the Galactic magnetic field on large scales [Vanderwoude et al., in press]. However, they only mapped the northern sky, and so far the southern sky has been poorly sampled. Progress in finding RMs per cluster has gone from 1-2 measurements per

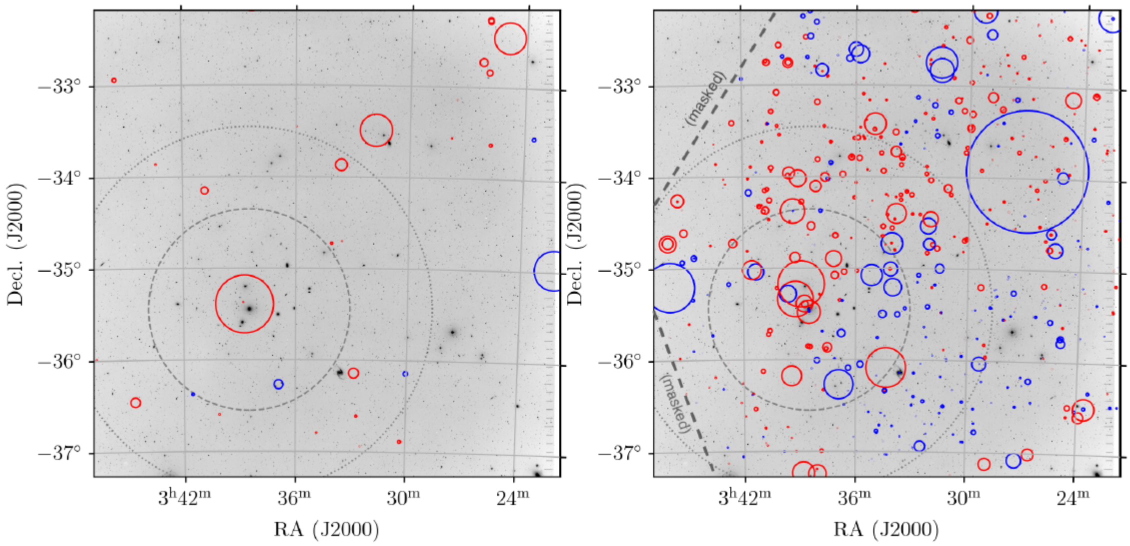

Figure 2.2: This figure is taken from Gaensler et al. [submitted] and is a good representation of the progress in RM grids. The outer dotted circle represents the virial radius of the Fornax cluster. The left side shows the RM grid from NVSS data. The right side shows an equivalent RM grid from POSSUM. Red indicates positive RMs and blue indicate negative RMs. The uncertainties on ASKAP RMs are also usually an order of magnitude smaller than the NVSS RMs.

cluster before POSSUM to now obtaining tens to a few hundreds. This progress in using RM grids to study galaxy clusters has been hindered by a lack of detail of the foreground contribution and bad sampling of polarisation data which has led to incorrect RM fits [Johnston-Hollitt et al., 2015]. Anderson et al. [2021], which used early commissioning data for the POSSUM survey, and for the first time, searched for Faraday RM enhancements to trace the structure of magnetised ionised gas in a low-mass galaxy cluster. They found that the Faraday depth enhancements extends 2-4 times the projected distance from the X-ray emitting ICM. RM grid techniques to study the ICM or Warm-Hot Intergalactic Medium (WHIM) in individual galaxy clusters have previously been challenging due to the low density of polarised sources and the uncertainty of whether the RM grid source was located behind, within, or in the foreground of the target cluster [Anderson et al., 2021]. However, with new radio instrumentation, ASKAP can measure polarised source densities of around 25 per square degree. Therefore, in observational galaxy cluster astrophysics, POSSUM will invite routine RM grid studies.

2.5.1 Dispersion of RMs in Clusters

As shown in Figure 2.3, it is expected that the RM dispersion in clusters decreases with distance from the cluster centre. However, at the time of Johnston-Hollitt et al.

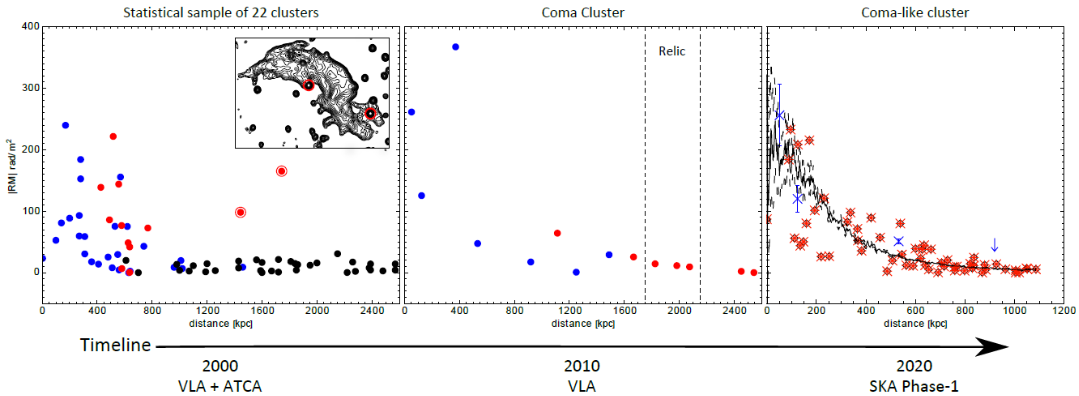

Figure 2.3: The right panel shows the current expected statistical RM dispersion in galaxy clusters from Johnston-Hollitt et al. [2015]. The figure shows the improvements in RM detection over time from only having a statistical sample of 22 clusters to 10 RMs per cluster to several tens of RMs per cluster in the present era.

[2015], they had little information on the extent of the magnetic fields in clusters, and their influence on cluster dynamics, particularly in the outskirts. Since there has been significant progress in statistical observations of RMs in galaxy clusters, it is crucial to test if observations match the expectations of RM dispersions in cluster outskirts.

2.6 Peripheral Gas of Clusters

The extended region of galaxy clusters is believed to contain hot, diffuse, X-ray emitting plasma. This region hosts the majority of the diffuse gas in these systems and contains the complex physics involved in large-scale structure growth [Simionescu et al., 2021]. These processes are believed to be different to the physics occurring in the cores of galaxy clusters that has been the main focus of observations. Studying the contents of the cluster outskirts would help our understanding of the overall growth of galaxy clusters and their connections to the Cosmic Web. The matter in the extended regions has been heated by strong structure formation shocks and during the formation and evolution of galaxy clusters shocks occur. One type are accretion shocks, caused by the deceleration of infalling baryons, or when low-temperature, low-density gas accreting from void regions is heated to X-ray emitting temperatures with high Mach numbers [Zhang et al., 2020]., [Simionescu et al., 2021]. This is the outermost boundary of the X-ray emitting gas halo of galaxy clusters [Simionescu et al., 2021]. Another type are merger shocks which are caused by a large enough infalling subcluster moving away from the main-cluster centre. Zhang et al. [2020] argue that when the merger shock overtakes the accretion shock, a new and longer lasting shock is formed that travels beyond the virial radius of the main cluster which affects the cold gas around the cluster. Despite these shocks being responsible for heating most of the baryons in the Universe, neither have been probed before observationally [Simionescu et al., 2021]. We need direct measurements of the entropy profile beyond the virial radius of clusters to understand the heating of the ICM.

Ilani et al. [2024] recently detected a "highly significant" excess of X-ray and radio catalogue sources that were stacked around MCXC galaxy clusters, near and beyond the virial shock radius. They suggest that the properties of the excess sources make it likely that they are not AGN or background sources and are instead infalling gaseous clumps interacting with the virial shock. They believe these are galactic halos and outflow remnants. If this claim were true it would be quite remarkable, and would also require care when using POSSUM RMs, requiring us to establish that the sources are truly in the background of the clusters. Conversely, if true, it could also provide a new means of probing intergalactic gas.

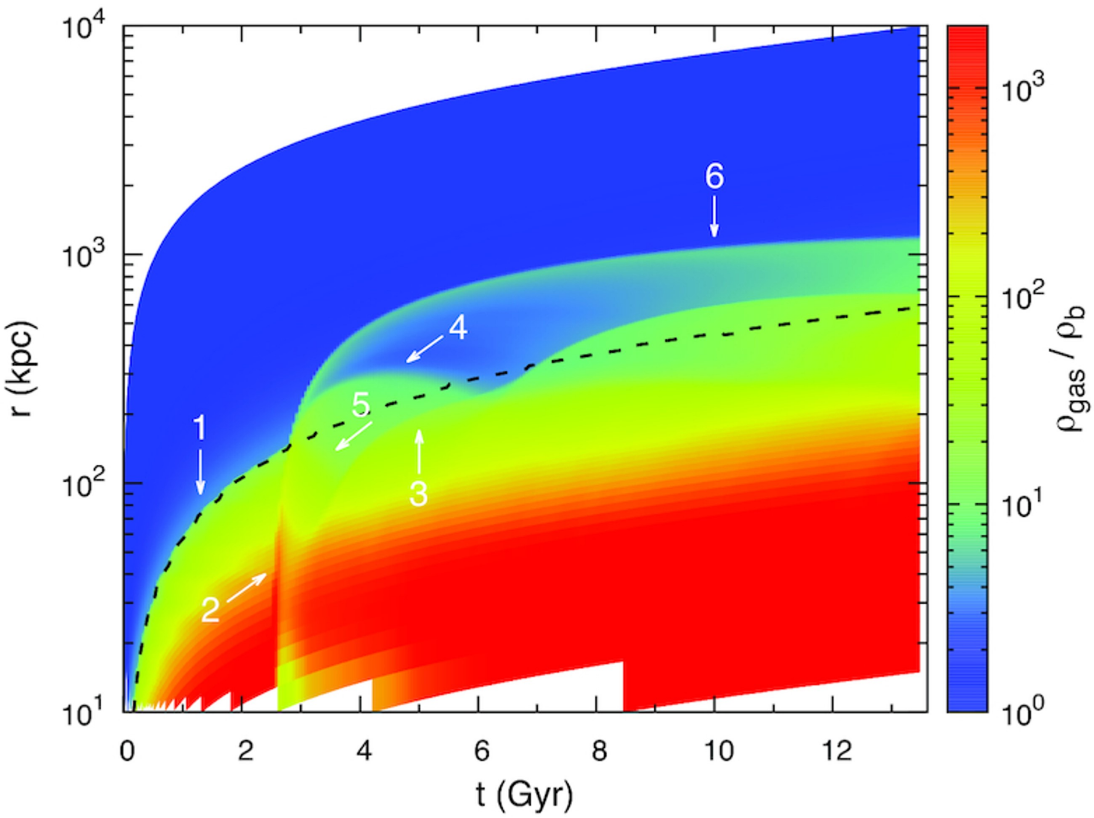

Figure 2.4: Evolution of the gas density profile a simulation by Zhang et al. [2020] showing shocks travelling beyond the cluster virial radius (the black dashed line).

2.7 Summary

Polarimetry and RMs are powerful tools for studying cosmic magnetic fields. POSSUM and ASKAP represent a revolutionary step forward in our ability to measure these RMs and construct dense RM grids. The peripheries of galaxy clusters are sites of important astrophysical processes, but current methods of observing the intracluster medium (e.g. X-rays) are insufficient to fully capture them. The dense RM grids provided by POSSUM offer a potential new window into these processes. In the next few chapters, I will perform the first ever experiments using RM grids to search for gas at the periphery of galaxy clusters.

Chapter 3

Methodology

3.1 Experimental Design

While RM grid experiments are conceptually simple, the POSSUM RM grid stands out by incorporating decades of advancements in best-practice imaging and calibration techniques. Additionally, it contains hundreds of times more information compared to previous large-area RM grid surveys such as NVSS. In the following sections, I describe the experimental setup and data processing in detail.

The ASKAP observatory maintains and operates the ASKAPsoft pipeline which performs interferometric calibrating and imaging, producing images, data cubes, and other products for observations of each 30 square degree, 36 beam observing footprint. The instrumental bandpass is derived from observations of the unpolarised calibrator source PKS B1934-638, and the on-axis leakage spectra for each antenna and formed beam [Gaensler et al., submitted]. After this is applied to the data, the time-dependent gain variations for each beam are obtained using a single amplitude and phase self-calibration iteration. The on-axis instrumental leakages from this calibration is corrected to better than 0.1% of Stokes I [Gaensler et al., submitted].

The ASKAPsoft pipeline then images the data to produce Stokes IQUV spectral cubes. It does so by first generating images for each of the 36 formed beams and linearly mosaicking them to form a set of image and cube products for each ASKAP observing footprint. Holographic observations of the point source PKS B0407-638 are used to obtain the full-Stokes models of the primary beam to correct for the off-axis leakage of the Stokes I, Q, U and V, and for the sensitivity pattern of the primary beam. State final leakage accuracy over the field is better than 0.2% of Stokes I into Stokes QUV, and no other GHz-band interferometer in the world can come within an order of magnitude of this accuracy over wide fields. This uniquely enables the experiment that I pursued.

Source finding is then run on the Stokes I full-band mosaics, which produces a list of positions of total intensity source components [Gaensler et al., submitted]. The Stokes IQUV spectra are then extracted at the location of each source component, and the RM is calculated from the resulting IQU spectra for each source. The RMs for all POSSUM observations taken to date were downloaded from The CSIRO ASKAP Science Data Archive (CASDA), which is where data from POSSUM is archived. For each deposited data set, members of the POSSUM Collaboration evaluate whether this data meets a series of quality control benchmarks. If so, the data is released to the public, which contains as a key data product, a raw catalog of RMs and their positions on the sky.

3.2 Further Data Quality Evaluation

Since the POSSUM collaboration is still working on understanding data quality, I performed a visual inspection to look for obvious issues. In so doing, I identified issues affecting one specific observation in my sample. For the observation containing cluster Abell 3667, there are coherent patches of positive and negative RMs, and patches with no RMs, as seen in Figure 3.1. These patches of RMs have a similar size across the field, which distinguishes them from the coherent patches that constitute my main results. Consultation with POSSUM experts suggests that this is most likely due to foreground diffuse polarised synchrotron emission from the Galactic interstellar medium (ISM). However since the ISM emits polarised emission and Faraday rotates it, this is not something that can be corrected with the surrounding background RMs in foreground subtraction. The only method to correct this is with a more advanced experimental method in the POSSUM pipeline, and given that this only appears to affect a single object, I have decided to simply discard it. My final sample is explained in 3.3. However, fields like this will serve as a valuable testbed for the 'diffuse emission subtraction' correction techniques that POSSUM is developing. It should be noted that other clusters in my sample are also potentially affected by this issue, and this possibility is mentioned as a caveat in Chapter 5 when I interpret the results of this thesis.

3.3 Sample

My sample selection was guided by the goal of investigating gas at the periphery of massive galaxy clusters using POSSUM RMs, as previously described. Therefore, a key criterion was selecting clusters with at least tens of RMs passing through these outer regions, ensuring enough data points for a statistical detection of elevated $|RM|$ values. I selected suitable clusters as follows:

1. Contained in either or both of the biggest current X-ray catalogues, the meta-catalogue of X-ray detected clusters of galaxies (MCXC), and the RASS-based X-ray selected extended Galaxy Clusters Catalog (RXGCC). If contained in these catalogues it implies that they are known to host hot gas.

2. Weighs at least 10^{14} solar masses to be considered a cluster.

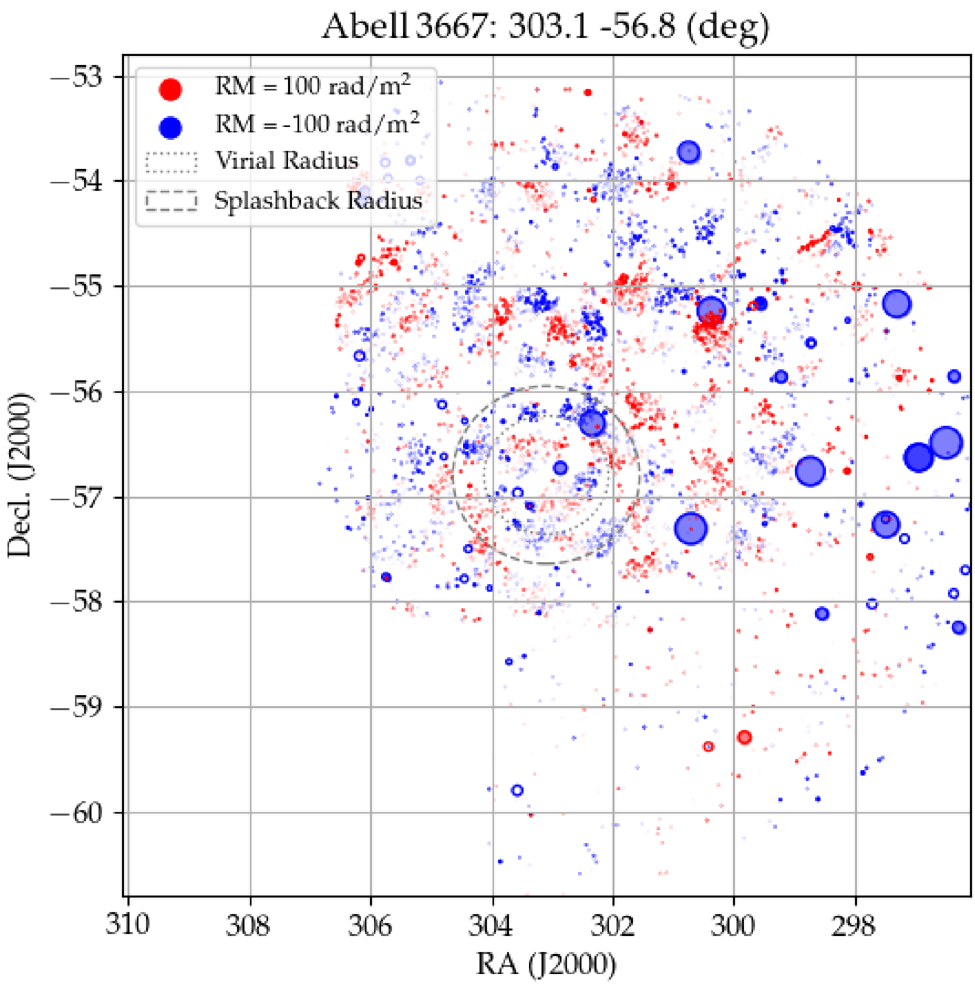

Figure 3.1: Cluster Abell 3667 shows data quality issues with coherent patches of positive and negative RMs. Blue indicates negative RMs and red indicates positive RMs. These patches extend far beyond the splashback radius which points to it being due to diffuse emission in the foreground.

3. Infall region sky area of at least 1 square degree in order to obtain tens to even hundreds of RMs through the region outside the virial radius.

4. Not too large on the sky for Galactic foreground RM correction to be a concern. If, however, the clusters were too large on the sky, they could overlap with large-scale Galactic structures which would be difficult to subtract.

For the resulting prospective objects, I cross-matched their positions with POSSUM RM coverage. There were 10 sources selected as targets for this project, with one of these discarded due to data quality issues as mentioned in 3.2, and three of these removed due to a lack of RM coverage when I subtracted RMs within 10 degrees of the Galactic plane, Large Magellanic Cloud (LMC), and Small Magellanic Cloud (SMC) (see next paragraph). Table 3.1 lists the final sample of clusters, including their names, right ascension, declination, virial radius in degrees, infall area in square degrees, and their mass in $10^{14}M_{\odot}$.

Cluster Name	RA (J2000)	Dec (J2000)	Virial Radius (deg)	Splashback Radius (deg)	Cluster Mass ($10^{14}M_{\odot}$)
Triangulum Australis	249.57	-64.35	0.622	0.932	5.24
Abell 1736	201.73	-27.18	0.556	0.834	2.71
Abell 3391	96.59	-53.69	0.480	0.720	2.16
Abell 3266	67.85	-61.42	0.552	0.829	4.56
Abell 3581	211.87	-27.02	0.835	1.25	1.08
MKW 8	220.16	3.47	0.721	1.08	1.15

Table 3.1: My final sample of clusters including their names, coordinates, virial radius, splashback radius, and mass.

As mentioned above, the current best catalogues of clusters with clear evidence of a hot gas ICM are the MCXC and the RXGCC. Once MCXC and RXGCC clusters were chosen subject to the selection criteria (as stated above), the clusters were cross-matched with POSSUM observations. The POSSUM survey coverage was checked against a list of positions to give a list of the scheduling block IDs (SBIDs) of POSSUM observations that corresponded to each position. The data also underwent de-duplication for RMs in regions with overlapping tiles. Sources are considered duplicates if they have positions within 3 arcseconds of another which is the astrometric accuracy of ASKAP. I also filtered out data that was within 10 degrees of the Galactic plane, the LMC and the SMC. This resulted in some clusters being filtered out due to their location on the sky. I note that some of the clusters in my sample were not completely covered by POSSUM data. While I have decided to still include them in my sample, I have visually inspected the coverage percentage for each cluster, and this was taken into account in analysis.

3.4 Galactic Foreground Subtraction

Faraday rotation can occur in any reservoir of magnetised plasma along the line of sight to a polarised radio source. In practice, one of the main contributors is the magnetised ISM of the Milky Way Galaxy, whose contribution needs to be removed in order to study Faraday rotation of objects in the background. Galactic foreground subtraction is necessary in order to remove the Faraday rotation from the Galactic foreground, and to determine whether Faraday rotation enhancements seen in RM grids are Galactic in origin or indeed due to the galaxy clusters. Figure 3.2 and 3.3 show the pre-foreground-corrected RMs and the post-foreground-corrected RMs respectively. The positions of each of the clusters in my sample are marked on the figures.

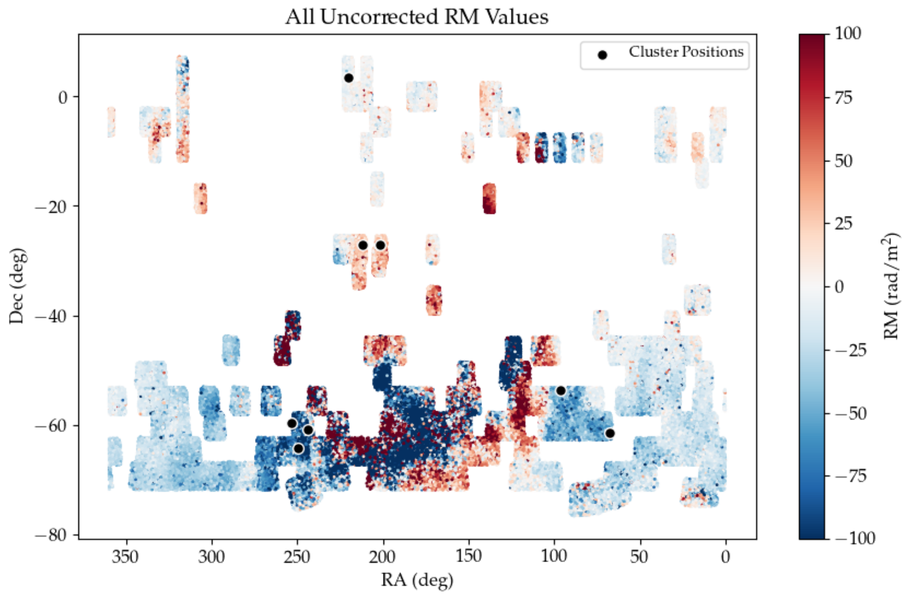

Figure 3.2: All POSSUM RMs that have not yet gone through galactic foreground subtraction. The positions of each of the clusters in my sample are marked with the black circles.

Since the Galactic ISM foreground is expected to vary relatively smoothly to first order on degree scales [Anderson et al., 2024], the effect of this structure (the 'foreground RM') can be subtracted from the observed RM to produce the residual RM, or RRM. To achieve this, annular regions were selected for each RM, and RMs within this 'exclusion radius' were removed so that potential spatially correlated signal due to the contribution of the cluster ICMs was not subtracted out. To compute the correction, a chosen number of nearest RMs (excluding those within the exclusion radius) were selected for each RM, and the median of these RMs was the estimate for the Galactic foreground. All the RMs were then corrected by subtracting the median

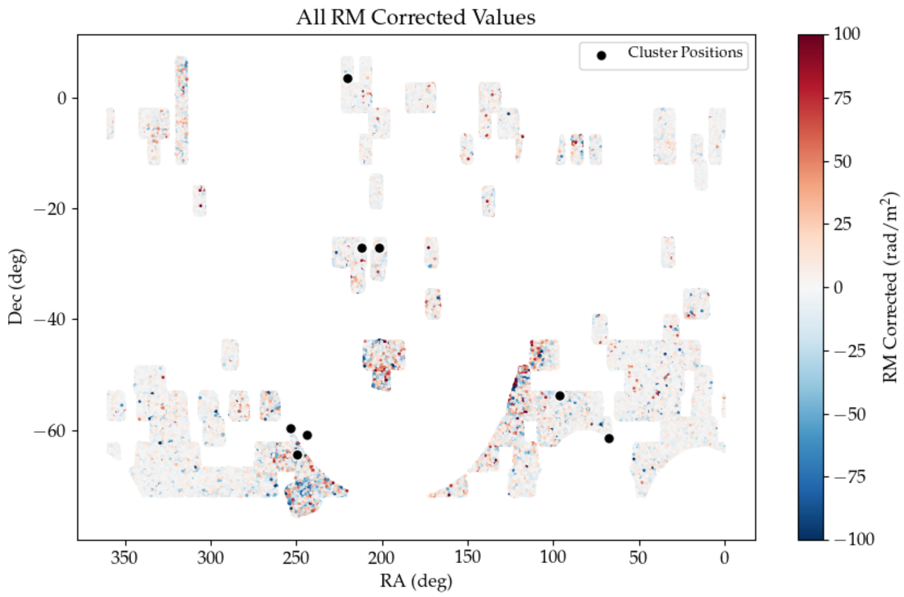

Figure 3.3: All POSSUM RRMs that have already gone through galactic foreground subtraction. Some outlier RRMs are visually apparent as isolated large |RRM| values. The positions of each of the clusters in my sample are marked with the black circles.

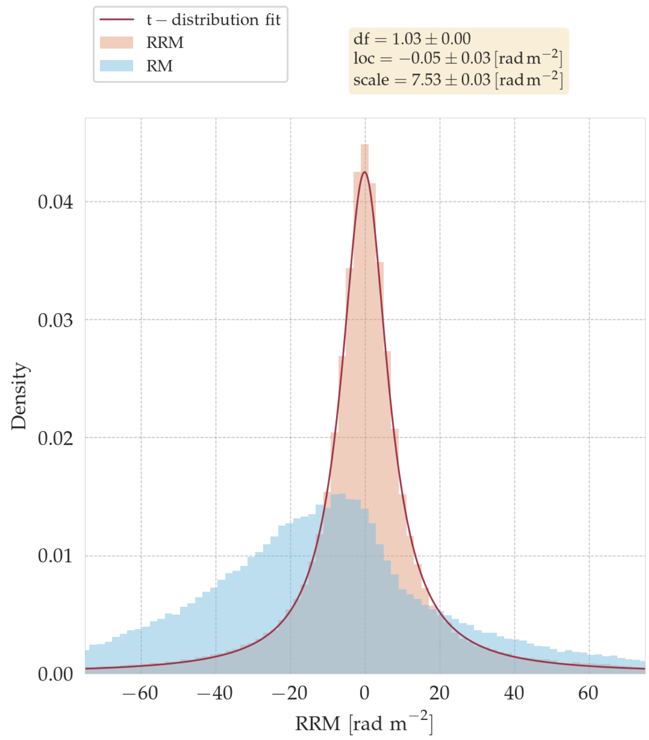

Figure 3.4: Histograms of RM (blue) and RRM (orange) for all POSSUM RMs. The bin values for RRMs were fitted with a Student's t-distribution (red line). The best-fit parameter values are listed in the yellow text box where the 'df' param is proportional to the tail of the distribution, the 'loc' is the fitted centre of the distribution, and the 'scale' is similar to the standard deviation or measure of the spread of the RMs.

from each RM. The exclusion radius was set to 0.4 degrees and the nearest number of RMs was set to 40 as done in Anderson et al. [2021].

Figure 3.4 shows histograms of uncorrected RMs and residual RMs (RRMs) which are the Galactic RM foreground subtracted RMs. The RRMs were fit by a Student t-distribution and the degrees of freedom (df) which is proportional to the tails of the distribution is 1.03 ±0.00, the location of the fitted centre of the distribution is -0.05 ±0.03 rad/m/m, and the scale or measure of the spread of the RMs is 7.53 ±0.03 rad/m/m. Since the df value is close to 1, it indicates tail-heavy distribution with outliers, as expected in Taylor et al. [2009]; Schnitzeler [2010]; Arámburo-García et al. [2021]; Thomson et al. [2023]. The scale value aligns with extragalactic point source RM dispersion measurements done by Taylor et al. [2024]. However, it is slightly higher than measurements done by Schnitzeler [2010]. Therefore this correction has matched most expectations, and has successfully subtracted the Galactic foreground.

Chapter 4

Analysis and Results

4.1 Visual Identification of Coherent RM Features and RM Outliers

Representations of the RM grid associated with each of the clusters in my final sample are shown in Figures 4.1 and 4.2. As a first step in my analysis, I visually inspected my sample for coherent variations, features, or outliers in the spatial distribution of RRMs, which might indicate the presence of magnetised gas, or coherent RM patterns potentially linked to phenomena such as shocks, within or beyond the cluster infall regions.

For clusters Abell 3266, MKW 8, and Abell 3581 there are individual polarised sources with |RRM| values that are clearly strongly elevated above surrounding RRMs in the vicinity of the infall region. However, there is also similarly elevated isolated sources well beyond the infall region. From visual inspection, it is unclear whether the elevated RRM values are more concentrated near the infall region. In sections 4.2 and 4.4, I test this numerically.

Three of the clusters exhibit notably unusual RRM structures compared to typical extragalactic regions. The Abell 1736 cluster has a feature of coherent positive RRMs to the northwest beyond the splashback radius, however since they do not overlap with the infall region and are not substantially large, I chose not to focus on this in further analysis. The Abell 3391 cluster appears to have an extraordinarily large RRM value at a right ascension and declination of (99.38, -53.69) degrees or 2.07 degrees beyond the splashback radius, with another substantial RRM value north of the cluster close to the splashback radius. The Triangulum Australis cluster shows an RM grid with a variety of structure, with coherent patches of elevated |RM| values within and beyond the infall region. Specifically, there is a coherent band of negative RRMs from the infall region, about 0.3 degrees wide, extending $\approx$ 1.5 degrees roughly northeast from the indicated splashback radius boundary. There are other smaller patches of similarly large RM values located at the splashback boundary to the south of the cluster, and to the west, just inside the virial radius. There were also to the east, well outside the splashback radius, a patch of coherent positive RRMs that could be associated with the cluster. However they did not overlap with the infall region and so were not a component of further analysis. Two patches of particular interest are shown in Figure 4.3, and form the basis for more in-depth analysis presented in Sections 4.2, 4.3, and 4.4. Figure 4.4 shows a Voronoi plot of the Triangulum Australis cluster, highlighting the relationship between the |RRM| enhancement and the surrounding, more typical RRM values with greater clarity. A Voronoi plot is created by dividing up an area into tessellating polygons around individual points of interest (here, individual RRMs) with the boundaries based on the distance to the points around it. The RRM enhancements near the infall region (features) are clearly seen. These features in the Triangulum Australis cluster and the Abell 3391 cluster are a component of further analysis in this chapter, and it is determined whether these RRM variations are on the order of, or exceed, approximately 10 rad/m^2, which is what is expected for merger shocks and accretion flows in clusters [Bonafede et al., 2013].

4.2 Statistical Search for Radial and Azimuthal RM Enhancements

Naively, I would expect the highest |RRM| values in the roughly spherical cluster core [Clarke et al., 2001], where gas is in approximate hydrostatic equilibrium within the massive gravitational potential of the galaxy cluster. Moving from the cluster core to the periphery, where asymmetrical shocks and filaments connect to the filamentary cosmic web, I hypothesised that I would observe localised RRM enhancements against a broader trend of decreasing magnitude with radius, and increasing deviations from spherical symmetry in any RRM enhancements that I may observe. In this section, I employ statistical analysis to search for evidence of these features.

To both identify and quantify more subtle RRM enhancements than is possible with visual inspection alone, I calculated the spread or dispersion of RRM values in several radial bins with respect to the cluster centre, and separately, several azimuthal bins with respect to the cluster centre, as explained below. To calculate the RRM dispersions, I computed the median absolute deviation (MAD) for each specific region. The MAD is used as a measure of spread instead of the standard deviation because it is robust against outliers.

4.2.1 Radial Analysis

For the radial analysis, I calculated the MAD of RRM values located inside the virial radius, the infall region, and beyond the splashback radius out to 4 degrees from the cluster centre. Four degrees was chosen as this value is approximately 2-4 times the splashback radius and is the typical distance to the edge of an ASKAP field from a cluster contained therein. Since matter density decreases rapidly with radius past the splashback radius, selecting $\approx 4\times$ splashback radius as the boundary for this

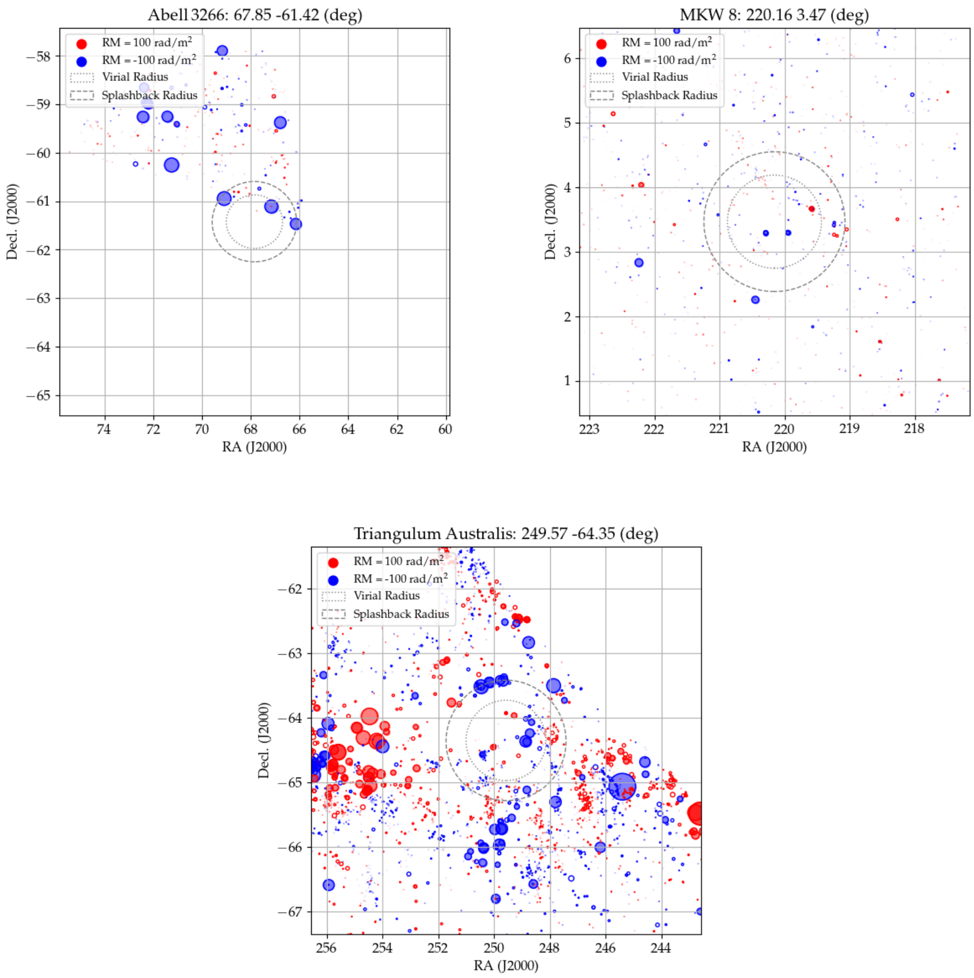

Figure 4.1: Each cluster is shown with the dotted line representing the virial radius and the dashed line representing the splashback radius. The area between these two lines is the infall region. The x-axis shows the J2000 right ascension and the y-axis shows the J2000 declination. The titles on each plot show the cluster name and the right ascension and declination in degrees of the cluster centre. Each RM is represented by a circle with blue as negative and red as positive. Filled in circles represent RM outliers defined according to criteria set out in Section 4.3. See the legend for a size and colour key for the RM values. The substantial RM value in Abell 3391 at 2.07 degrees beyond the splashback radius has a value of 1124 rad/m/m.

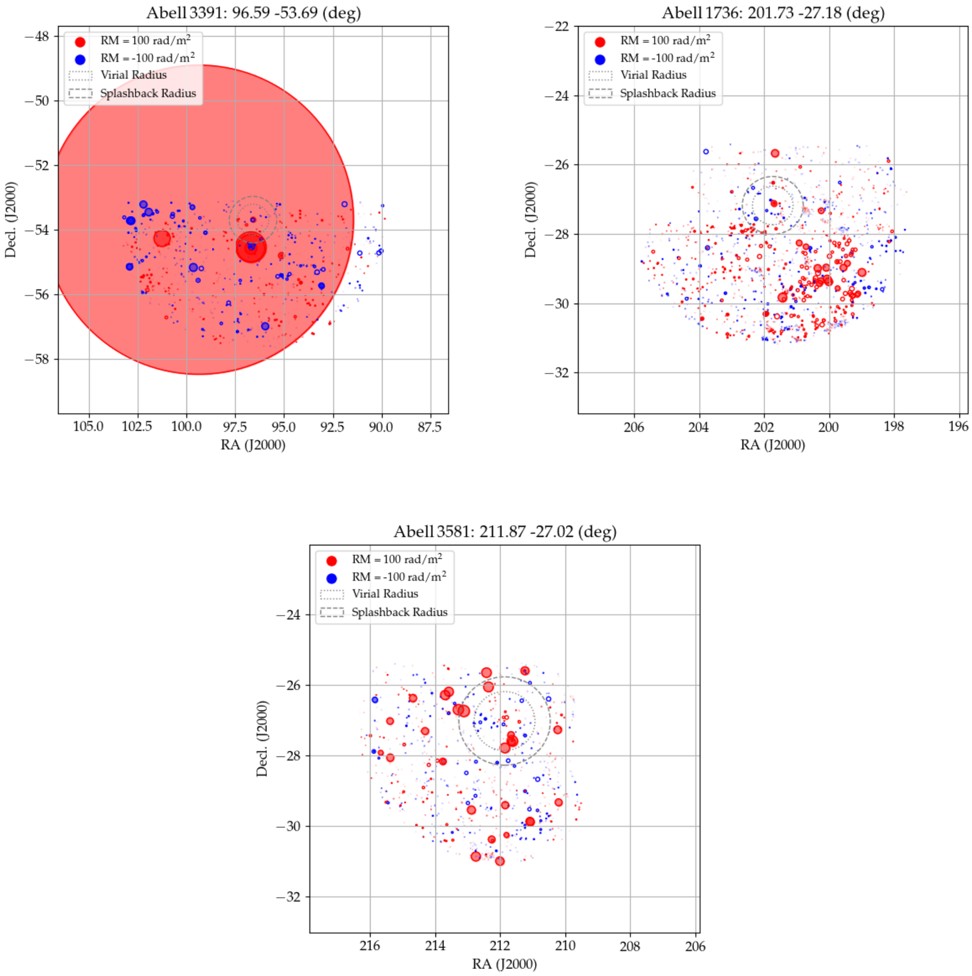

Figure 4.2: Continuation of Figure 4.1

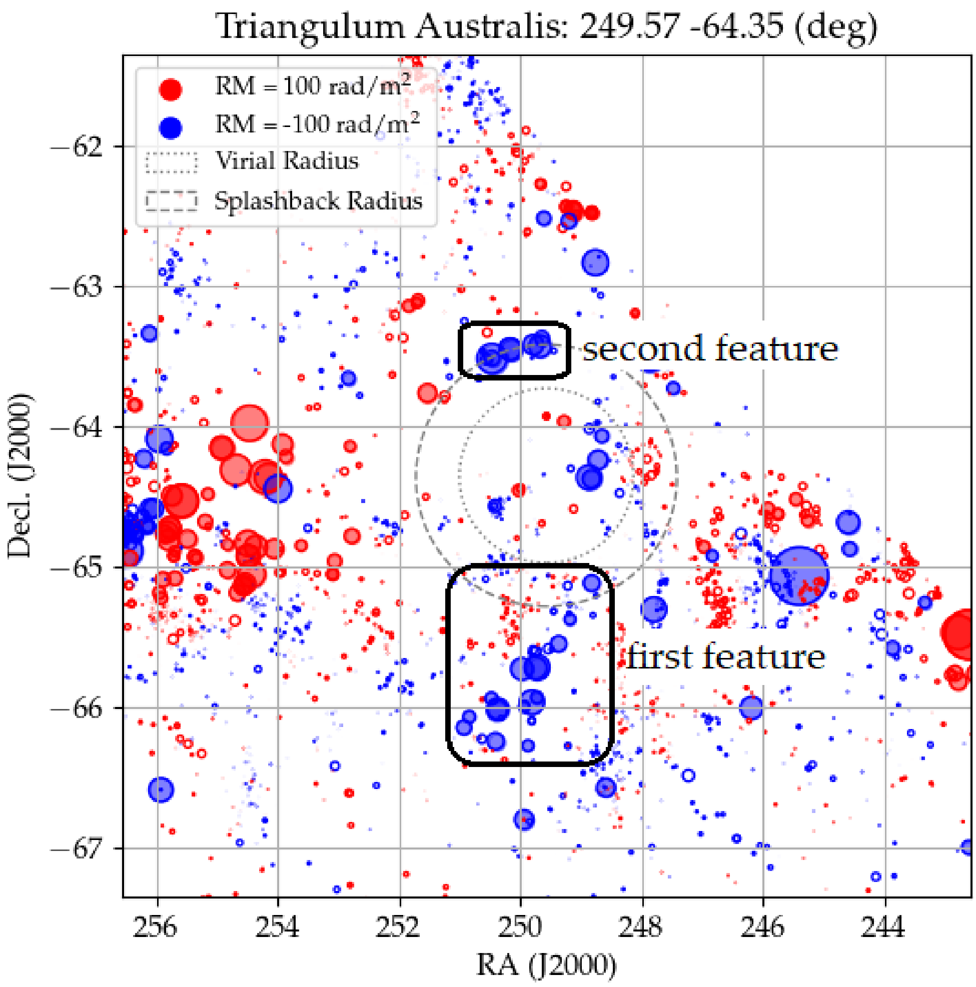

Figure 4.3: The Triangulum Australis cluster with each RM represented by a circle, where blue circles represent negative RMs and red positive RMs. Filled in circles represent RM outliers with the RMs masked according to the outlier criteria. The features of coherent RM patches of interest for this thesis are highlighted in black with labels.

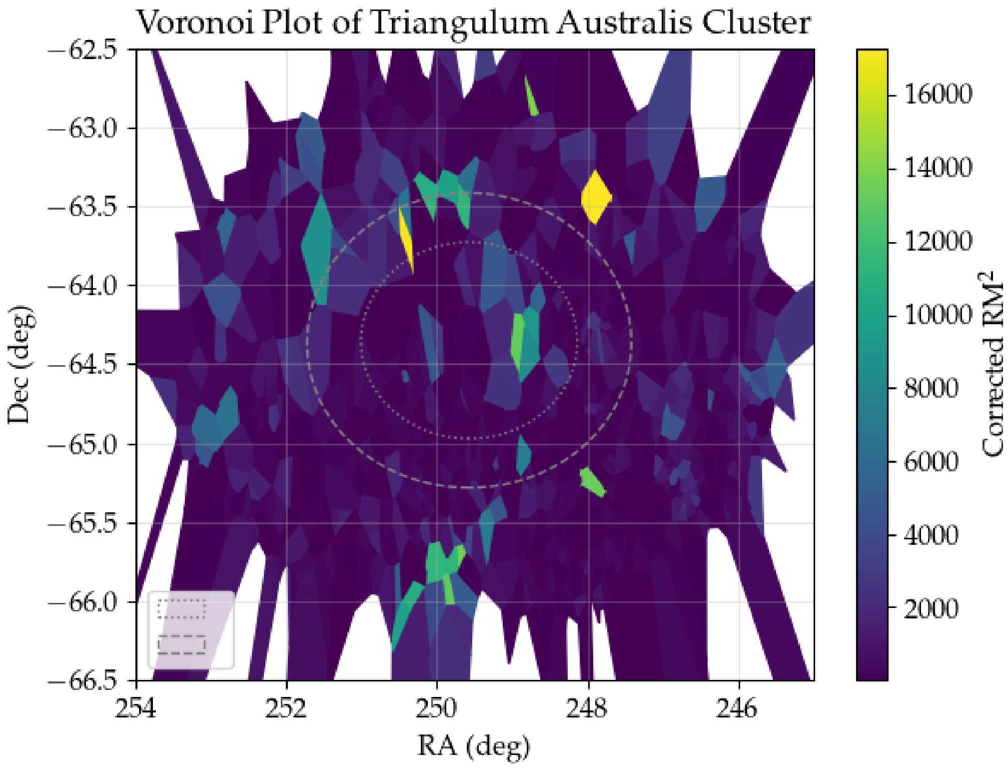

Figure 4.4: Image of the POSSUM Corrected RMs displayed in a Voronoi plot for the Triangulum Australis cluster.

region is reasonable. The results, listed in Table 4.1, show that the RRM dispersion increases outwards for the Triangulum Australis cluster and the Abell 1736 cluster, and the RRM dispersion seems to decrease outwards for the remaining four of the clusters in my sample. Finding an increasing RRM dispersion with cluster radius is unexpected given that there is typically a significant monotonic increase in the RM scatter closer to the cluster centres [Clarke et al., 2001; Osinga et al., 2024]. However Osinga et al. [2024] also observed that the RM scatter beyond the R_{500} radius (the radius enclosing an overdensity of 500 at the cluster redshift) was significantly higher than expected 5-7 rad/m/m intrinsic variation in typical polarised extragalactic radio sources [Schnitzeler, 2010; Taylor et al., 2024]. It should be noted that the Abell 3266 cluster has not been completely covered by POSSUM yet, which has affected the MAD calculations. This has been highlighted with an asterisk in the tables.

Cluster Name	Virial Radius (Mpc)	Splash-back Radius (Mpc)	Cluster Mass ($10^{14}M_{\odot}$)	Within Virial Radius (rad/m^2)	Infall Region (rad/m^2)	Beyond Splashback Radius (rad/m^2)
Triangulum Australis	2.53	3.80	5.24	17.8	19.3	23.6
Abell 1736	2.04	3.05	2.71	9.93	14.8	10.0
Abell 3391	1.89	2.83	2.16	16.7	7.88	14.2
MKW 8	1.33	1.99	1.15	8.46	6.29	5.26
Abell 3266*	2.41	3.62	4.56	17.6	14.9	8.09
Abell 3581	1.51	2.26	1.08	18.4	10.2	7.49

Table 4.1: The virial radius, splashback radius, cluster mass and the RM dispersion for each radial area of each cluster. The area beyond the splashback radius was cut off at 4 degrees from the cluster centre. Each value is correct to 3 significant figures. *Clusters that haven't been fully covered by POSSUM yet.

4.2.2 Azimuthal Analysis

For the azimuthal analysis I divided each cluster into quadrants aligned with the local RA and Decl. positive and negative direction offsets to get a basic understanding of possible asymmetry of the RRM enhancements. I found the RRM dispersion or MAD in each area. An illustration of the area of each region is shown in Figure 4.5 and the results of the MAD calculations are shown in Table 4.2. The boundary for RM measurements was again set to 4 degrees from the cluster centre. The results show for the Triangulum Australis cluster a mostly symmetrical dispersion apart from the first quadrant because it has not been completely covered by POSSUM in that section. This follows from what is visually apparent in Figure 4.1 as there are RRM outliers in every quadrant. For Abell 1736 there is higher dispersion in quadrants 3 and 4 which is where the outliers appear visually as seen in Figure 4.2. For Abell 3391, and the outlier seen in quadrant 2 in Figure 4.2, corresponds to the highest RRM dispersion. The rest of the clusters show mostly symmetrical dispersions since they have mostly uniform RRM outliers, or are not completely covered by POSSUM.

Cluster Name	Virial Radius (Mpc)	Splash-back Radius (Mpc)	Cluster Mass ($10^{14} M_\odot$)	Quad-rant 1 (rad/m^2)	Quad-rant 2 (rad/m^2)	Quad-rant 3 (rad/m^2)	Quad-rant 4 (rad/m^2)
Triangulum Australis	2.53	3.80	5.24	34.4	22.2	19.8	20.9
Abell 1736	2.04	3.05	2.71	6.70	6.02	12.9	10.6
Abell 3391	1.89	2.83	2.16	15.2	18.4	13.9	14.1
Abell 3266*	2.41	3.62	4.56	9.45	7.24	9.65	11.69
Abell 3581	1.51	2.26	1.08	7.638	9.18	7.27	8.87
MKW 8	1.33	1.99	1.15	5.86	5.14	5.08	5.42

Table 4.2: The virial radius, splashback radius, cluster mass and the RM dispersion for each quadrant area of each cluster. The area beyond the splashback radius was cut off at 4 degrees from the cluster centre. Each value is correct to 3 significant figures. *Clusters that haven't been fully covered by POSSUM yet.

4.3 RM Outlier Analysis

In Section 4.1 and in Figures 4.1 and 4.2, I identified clear RRM outliers, or regions of coherent RRM enhancements, associated with the Triangulum Australis cluster and the Abell 3391 cluster from visual inspection alone. In this section, I formalise the concept of an RRM outlier and conduct statistical tests to determine whether there are statistically significant increases in RRM outliers associated with cluster infall regions.

In order to determine if the infall regions of my cluster sample are associated with RRM enhancements relative to the typical RM source population, it was crucial that I test for how often RRM outliers occur in typical extragalactic fields not associated

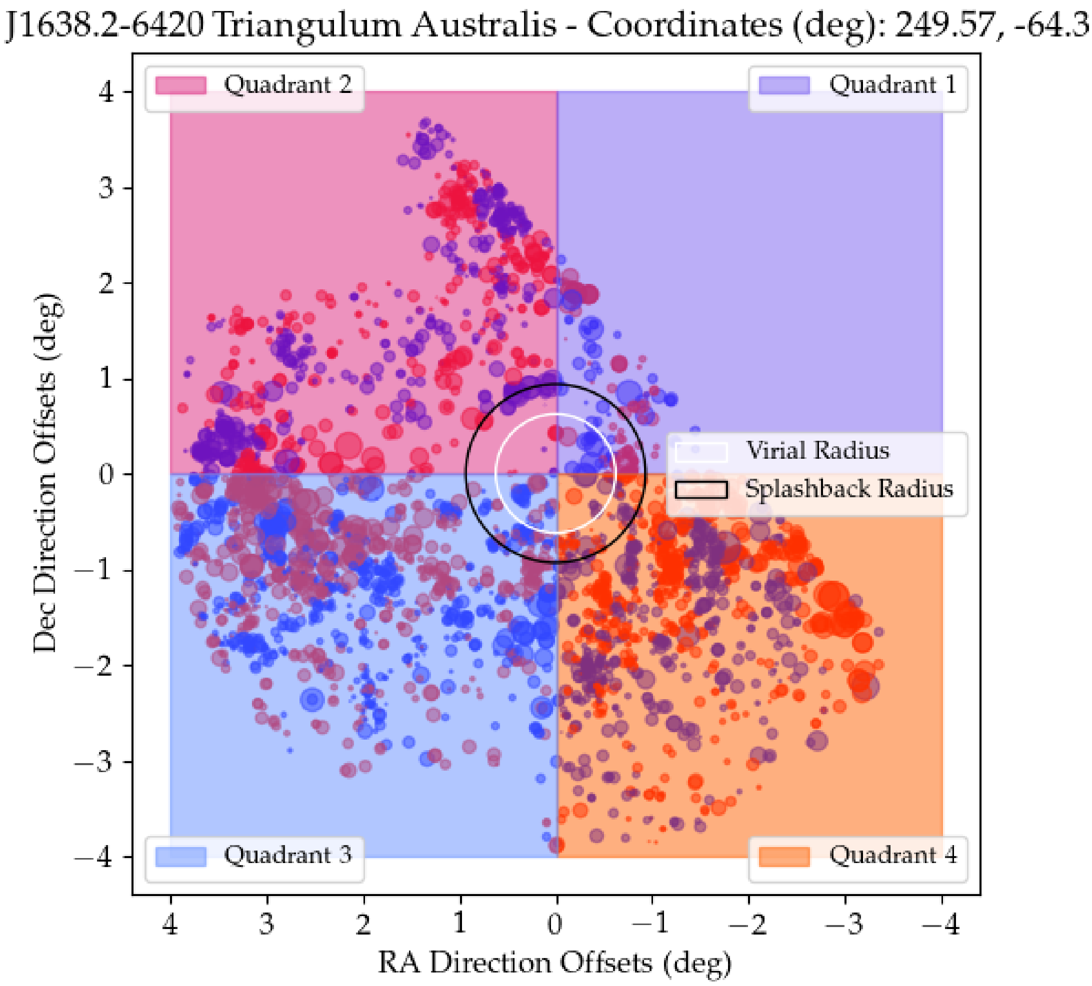

Figure 4.5: Triangulum Australis cluster illustration of the quadrant areas for the azimuthal analysis. The Median Absolute Deviation (MAD) was calculated for within 4 degrees from the cluster centre.

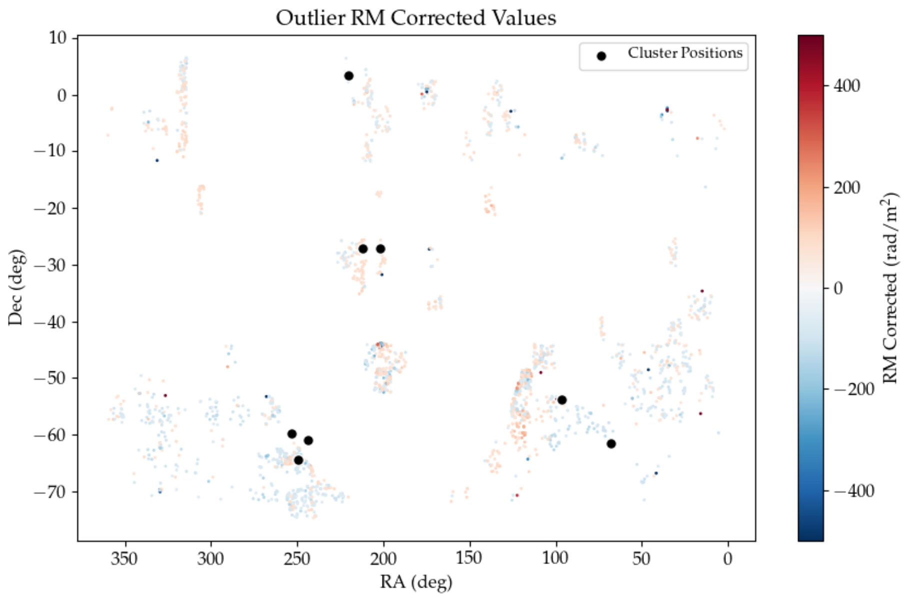

Figure 4.6: POSSUM RRM outliers from the total RMs that have gone through galactic foreground subtraction. The positions of each of the clusters in my sample are marked with the black circles.

with known galaxy clusters. To do this, the coordinates for all the POSSUM RMs to date were converted to galactic coordinates and sources that were within 10 degrees of the Galactic plane were masked out, along with RMs within 10 degrees of each of the Large and Small Magellanic Clouds. As shown in section 3.4 the corrected RMs are in a student t-distribution and so to select the outliers, a sigma threshold of 10 was chosen and a value of 6 rad/m^2 was chosen as the 1-sigma dispersion of the residual rotation measures (RRM) (or the foreground corrected) distribution for the corrected RM distribution. The value of 10 was chosen to ensure that the sources were clear outliers. I then calculated the quadrature sum of the RM uncertainties and the correction width for the RM distribution. Outlier RRMs were defined to be those having absolute values 10×the quadrature sum of the 6 rad/m/m and the RM uncertainty of the source. To determine the estimated number of outliers per square degree, the total number of outlier RRMs was divided by the total number of RRMs observed by POSSUM over the same area, and then multiplied by 35, which is the estimate for the number of RRMs per square degree [Vanderwoude et al., in press; Gaensler et al., submitted]. From this the estimated number of outlier RRMs per square degree was calculated to be ≈ 0.69. I made a visual inspection to ensure the outliers were clearly different from the rest of the population in terms of size and number. Figures 3.3 and 4.6 show all the POSSUM RRMs and the RRM outliers respectively.

I then sought to determine whether there is a statistical excess of outliers in the infall region of each cluster. Plotting the outliers for each cluster then revealed whether there were outliers in the infall region, and masking by simple logical conditions on the virial and splashback radii made it trivial to calculate the number of outliers per square degree in the infall region of each cluster. As mentioned in Section 3.3, some clusters were not completely covered by POSSUM and so this was taken into account by estimating the area covered in each cluster and using those areas in these calculations. To determine if the measured number of RRM outliers per square degree could be present by chance based on the density of outliers seen in typical non-cluster extragalactic fields, I used Poisson statistics. Under a Poisson distribution with the expected number of outliers per square degree (λ), the probability of k outliers per square degree is: $\frac{\lambda^k e^{-\lambda}}{k!}$. I found the probability of finding zero outliers per square degree, for example, to be ≈ 0.504, for one outlier per square degree to be ≈ 0.345 and for two outliers per square degree to be ≈ 0.118. The cluster infall regions in my sample are ≈ 1 square degree in size or greater.

Poisson statistics were applied separately each of the features of interest in the Triangulum Australis cluster (see Figure 4.3) since they are so visually striking (Section 4.1. For the first feature, as labelled in Figure 4.3, there are 16 RRM outliers and the feature area is 2.38 square degrees with boundaries determined visually. Therefore, for this first feature, there are ≈ 7 RRM outliers per square degree. Using Poisson statistics, the probability of 7 RRM outliers per square degree occurring by chance is 7.11×10^{-6}. For the second feature, as again labelled in 4.3, there are 8 RRM outliers and the feature area is 0.14 square degrees. Therefore, for this second feature, there are ≈ 57 RRM outliers per square degree. Using Poisson statistics, the probability of 57 RRM outliers per square degree occurring by chance is 5.61×10^{-87}.

4.3.1 Null Test: RM Outlier Density in Triangulum Australis vs. a Similar Galactic Latitude Patch

To further test whether the RRM outliers were due to the cluster or just by chance, I performed a null test on a random patch of sky covered by POSSUM at a similar Galactic latitude with coordinates (100, -60) ICRS degrees that was not overlapping any of the clusters in my sample. The null area is shown in Figure 4.7. The area of the null region was $16 \times 7 = 112$ square degrees, and there are 28 RRM outliers. This means there are 0.25 RRM outliers per square degree or 1 RRM outlier per 4 square degrees. Using Poisson statistics, the probability of finding 1 outlier per 4 square degrees is 0.18. It should be noted that the Triangulum Australis cluster was within $\pm$ 20 degrees of the Galactic plane, and $\pm$ 20 degrees masking is applied during outlier masking to ensure that RRMs are drawn from exceptionally clean extragalactic fields where the Galactic foreground correction is proven to work effectively. However, I expect that the $\pm$ 10 degrees masking to be sufficient. The other clusters in my sample that were not masked or removed from my sample due to Galactic foreground, the LMC or the SMC show a uniform spread of outliers with no similar structures that could be associated with infalling gas, which is what is seen in the null test for

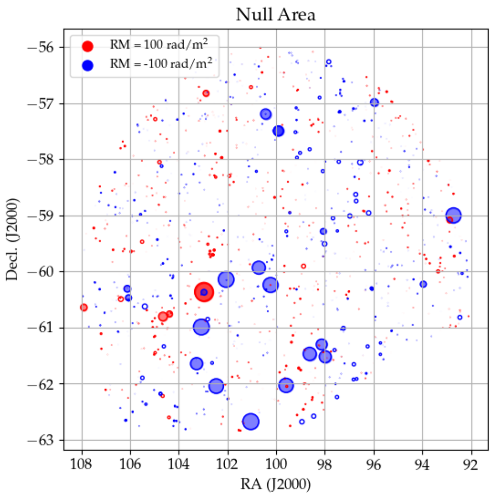

Figure 4.7: The null region at (100, -60) ICRS degrees that was not overlapping with any of the clusters in my sample, was in a region covered by POSSUM and at a similar latitude as the Triangulum Australis cluster. The x-axis shows the J2000 right ascension and the y-axis shows the J2000 declination. Each RM is represented by a circle with blue as negative and red as positive. Filled in circles represent RRM outliers with the RMs masked according to the outlier criteria. See the legend for a size and colour key for the RM values.

outliers.

In section 4.5 I show all POSSUM RRMs as a function of distance to the nearest cluster and these plots show that outliers tend to be closer to clusters. This means that I have a higher chance of finding RRM outliers in my cluster sample, and further suggests they are likely associated with the cluster itself.

4.3.2 Ripley's K Test to Assess Clumping of Outlier RRMs

To test whether the RRM outliers show statistically significant clumping on any particular scale, I implemented a spatial randomness test for the Triangulum Australis cluster and the Abell 3391 cluster. I used the Ripley's K function [Ripley, 1976] which iterates through each RRM outlier and counts the number of other RRM outliers within a given distance. The K function is the number of RRM outliers within a distance of a randomly chosen RRM outlier divided by the number per unit area of outlier RRMs. It can also be described as the mean nearest-neighbour distance or the cumulative distribution function of distance from random outlier RRMs to their nearest neighbours. The figures of the K function vs distance are shown in Figure 4.8. The spatial auto-correlation is found by analysing the positions of the observed line and the theoretical lines. When the observed line is above the theoretical line it indicates that there is clustering at that scale. When the observed line is below the theoretical line it indicates that there is even distribution at that scale. This analysis

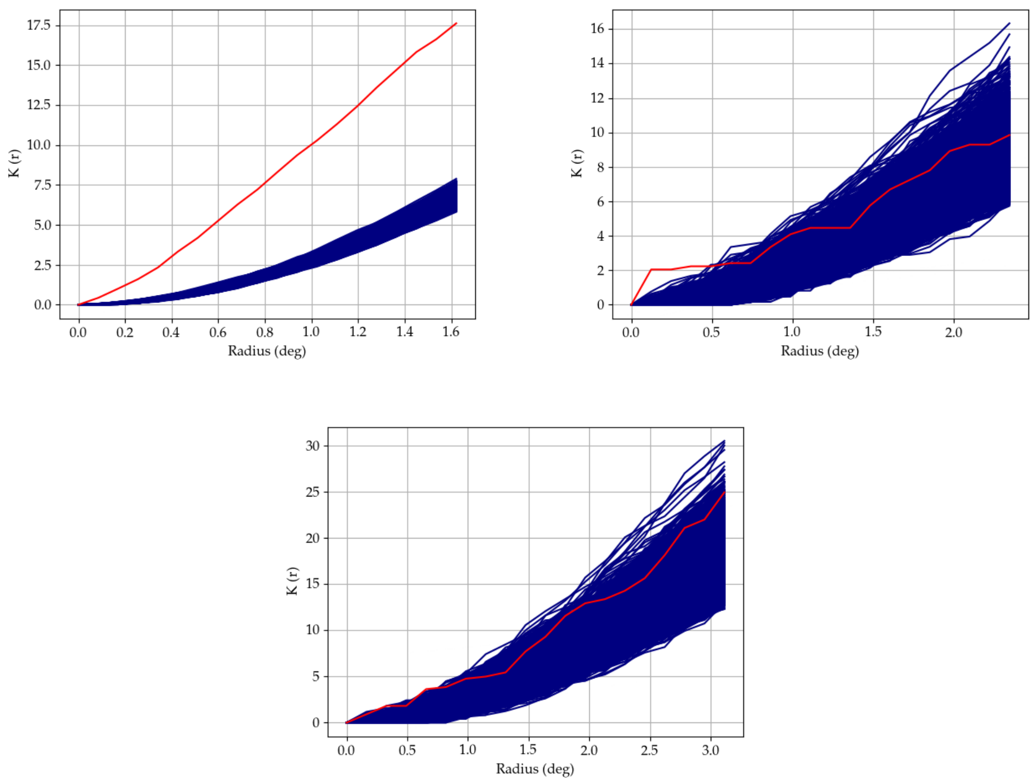

Figure 4.8: Plots of Ripley's K function, K(r) vs. angular separation radius for positions of RRMs. Top left is the Triangulum Australis cluster, top right is the Abell 3391 cluster and the last figure is the null area. The blue lines show the visualised output from the simulations which are what would be expected theoretically if points were randomly distributed across the area. The red line shows the observational data. Note the differing x-scales.

was performed for the entire cluster areas of the Triangulum Australis cluster and the Abell 3391 cluster, as well as for a null area with coordinates (100, -60) ICRS degrees as shown in Figure 4.7 and described in more detail in 4.3.1. As seen in Figure 4.8 Ripley's k test indicates that there is increasing clustering with increasing radius from the cluster centre for the Triangulum Australis cluster. The infall region for this cluster is between 0.93 and 0.62 degrees with the value of K(r) between 5-10 rad/m/m at these radii. The Abell 3391 cluster showed some clustering within the virial radius, however there was no clustering in the infall region. In comparison, the null test showed no clustering at all radii.

4.3.3 Kolmogorov-Smirnov (K-S) Test

To further evaluate the statistical significance of the outliers, I implemented the Kolmogorov-Smirnov (K-s) test to determine how likely the RRM outliers in the features from Section 4.1 are from the same RRM distribution as other samples of RMs. The two-sample K-S test evaluates the statistical significance of the differences in RM distributions between chosen samples. The K-S statistic quantifies a distance between the normalised cumulative distribution functions of the two samples. The null hypothesis of the K-S test is that the samples were drawn from the same distribution. The p-value here is the probability that the null hypothesis can be correct. I used the K-S test to determine whether the specific features in the Triangulum Australis cluster and the large RRM value seen in Abell 3391 cluster are statistically significant RRM enhancements. Figures 4.9 and 4.10 show illustrations of the K-S statistic with the cumulative distribution functions of two different RM samples. The distance between the two distributions is the K-S statistic. Table 4.3 shows the p-values and K-S statistics obtained from these tests. The p-values for all areas of comparison (except for the Triangulum Australis cluster with quadrant 1 and with quadrant 2 and for the Abell 3391 cluster with each quadrant) strongly support the rejection of the null hypothesis. This implies that there is asymmetry in the RRM distribution of the Triangulum Australis cluster and the Abell 3391 cluster and that the RRMs in the features (see Section 4.1) in both clusters are significantly different to the RRMs all other chosen areas of comparison. The cumulative distribution functions of the quadrants for the Triangulum Australis cluster and the Abell 3391 cluster clearly show different distributions for where the features are present in their respective clusters.

4.4 Comparison of RM Features to X-rays and Total Intensity Radio Emission

Overlaying total intensity radio emission (Stokes I) maps is a method of determining whether the asymmetrical RRM enhancements we have seen in the Triangulum Australis cluster and the Abell 3391 cluster are associated with imaging artefacts or diffuse radio structures that could be associated with shocks and infalling gas. For the clusters with increasing RRM dispersion with radius (particularly the Triangulum Australis cluster), it is worth investigating whether this matches the diffuse radio structures in the total intensity radio emission. The Stokes I maps were downloaded from CASDA for each cluster. Some clusters did not have a map that completely covered the cluster as the RMs were coming from an adjoining footprint. Mosaicking such data is complex and beyond the scope of this thesis, so I show the map most closely aligned with the cluster. This is the case for Abell 3391. Figures 4.11 and 4.12 show examples of the POSSUM RRMs overlaid on the Stokes I maps. For the Triangulum Australis cluster, there is no evidence for artefacts in Stokes I associated with the RRM enhancements. Moreover, there is evidence for diffuse emission in Stokes I in the infall region near the first feature (see Figure 4.3), and diffuse emission in the Stokes I that appears to be associated with the RRM enhancements in the second feature. For the Abell 3391 cluster, since the Stokes I map does not completely cover the cluster, it is unknown whether there is evidence for diffuse emission or artefacts in Stokes I associated with the RRM enhancements in this cluster.

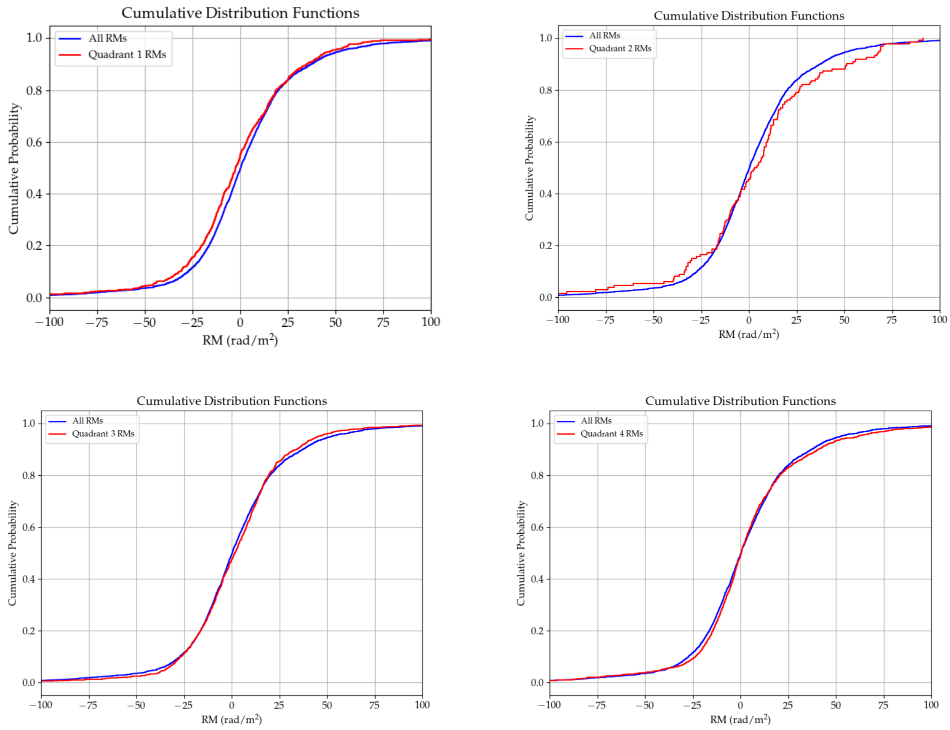

Figure 4.9: Cumulative Distribution Functions of all the Triangulum Australis RRMs and each quadrant's RRMs of the Triangulum Australis cluster.

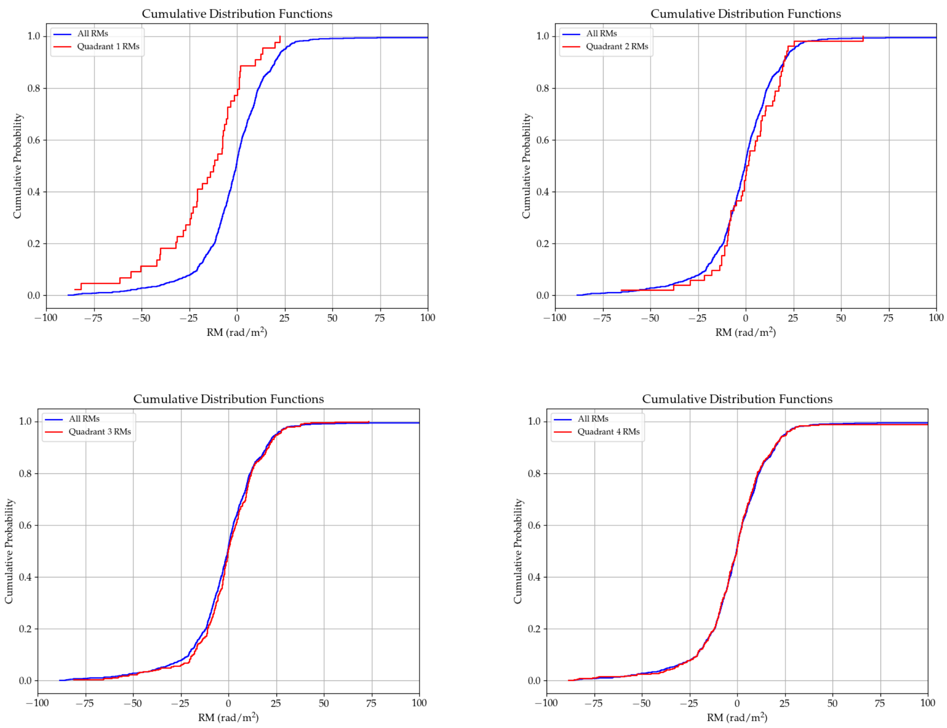

Figure 4.10: Cumulative Distribution Functions of all the Abell 3391 RRMs and each quadrant's RRMs of the Abell 3391 cluster.

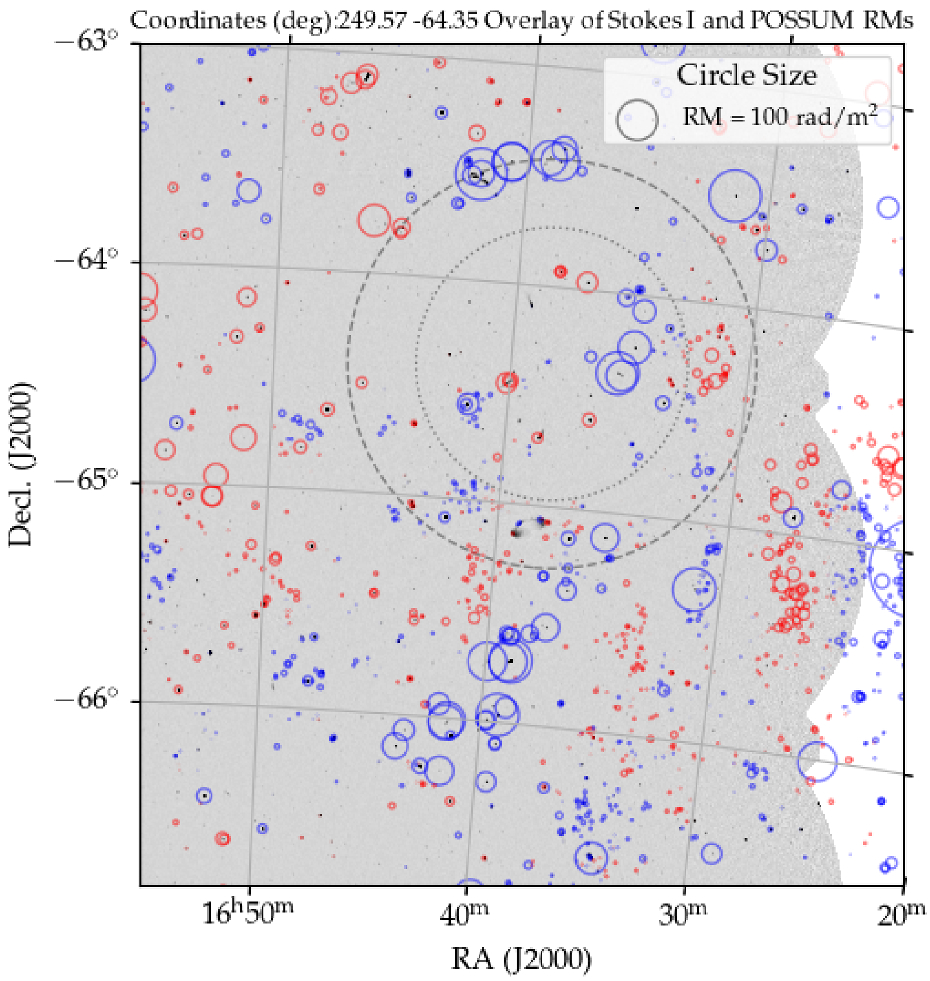

Figure 4.11: A figure of the Triangulum Australis Cluster with the POSSUM RRMs overlaid on the Stokes I map for that (grayscale) area. The dotted line is the virial radius and the dashed line is the splashback radius.

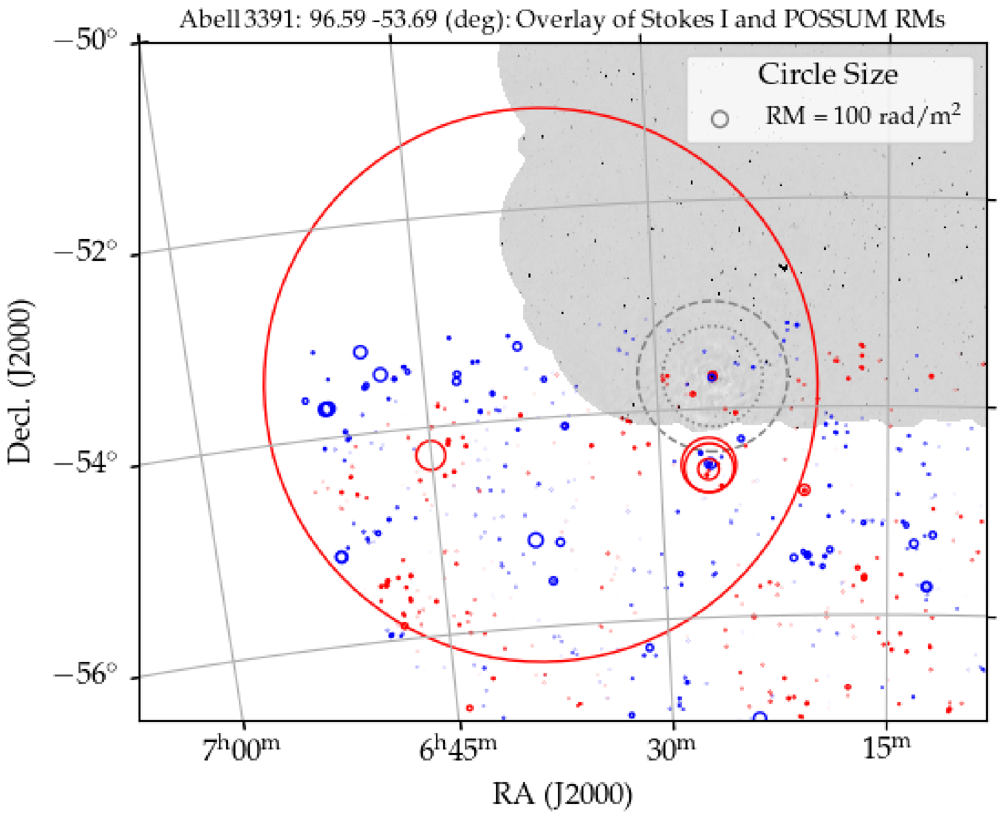

Figure 4.12: A figure of the Abell 3391 cluster with the POSSUM RRMs overlaid on the Stokes I map for that area. The dotted line is the virial radius and the dashed line is the splashback radius.

Areas of Comparison	P-value	K-S Statistic
Triangulum Australis and Null Area	3.88×10^{-59}	0.262
Triangulum Australis and All RM Data	9.18×10^{-285}	0.325
All RM Data and Null Area	3.97×10^{-14}	0.106
All RM Data and Abell 3391	6.04×10^{-30}	0.190
Null Area and Abell 3391	2.12×10^{-5}	0.100
Triangulum Australis and Feature 1	9.18×10^{-4}	0.109
Triangulum Australis and Feature 2	1.39×10^{-6}	0.581
All RM Data and Feature 1	5.61×10^{-45}	0.375
All RM Data and Feature 2	3.38×10^{-12}	0.767
Triangulum Australis Infall Region and Null Area	7.62×10^{-9}	0.249
Triangulum Australis Within Virial Radius and Null Area	3.13×10^{-6}	0.289
Triangulum Australis Beyond Splashback Radius and Null Area	1.35×10^{-58}	0.264
Triangulum Australis and Quadrant 1	0.0757	0.0543
Triangulum Australis and Quadrant 2	0.0629	0.115
Triangulum Australis and Quadrant 3	2.70×10^{-13}	0.0349
Triangulum Australis and Quadrant 4	6.57×10^{-14}	0.0465
Abell 3391 and Quadrant 1	0.0111	0.244
Abell 3391 and Quadrant 2	0.465	0.118
Abell 3391 and Quadrant 3	0.995	0.0247
Abell 3391 and Quadrant 4	0.999	0.0200

Table 4.3: Summary of Statistical Test Results from the K-S Test comparing different RRM samples. Results are quoted to 3 significant figures.

X-Ray observations as described in Section 2.4, have revealed inhomogeneous gas densities and large-scale structure filaments in galaxy clusters. Overlaying X-Ray images from eROSITA onto the POSSUM RRM outliers could help reveal infalling magnetised gas. As shown previously, the Triangulum Australis cluster is of particular interest due to tentative signs of infalling magnetised gas in the infall region evidenced by the RRMs. Figures 4.13 and 4.14 shows the X-Ray image for the Triangulum Australis cluster and the Abell 3391 cluster respectively from eROSITA sourced from the software Aladin with the POSSUM RRM outliers overlaid on the image. For the Triangulum Australis cluster there appears to be some asymmetry in the X-ray emission which implies that the cluster is disturbed. A disturbed cluster is usually associated with active accretion and dynamical shocks. For the Abell 3391 cluster, there is evidence of X-ray emission coincident with the RRM enhancements near the infall region [Simionescu et al., 2021]. The spatial coincidence of RRMs with this X-ray emission however suggests the emission is unlikely to be due to shocked gas, but rather spatially coincident galaxy clusters in their own right.

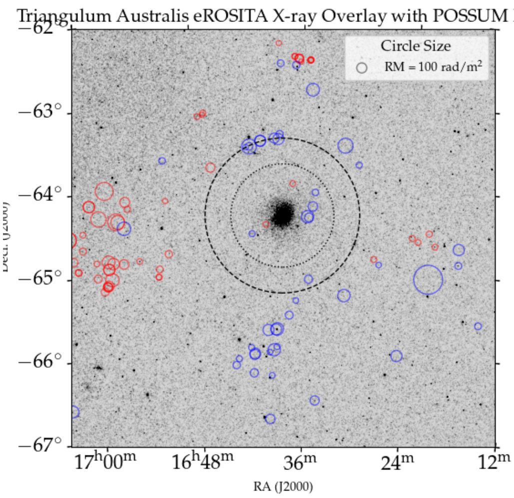

Figure 4.13: Image of the X-Ray data from eROSITA and the POSSUM RRMs overlaid on top for the Triangulum Australis cluster.

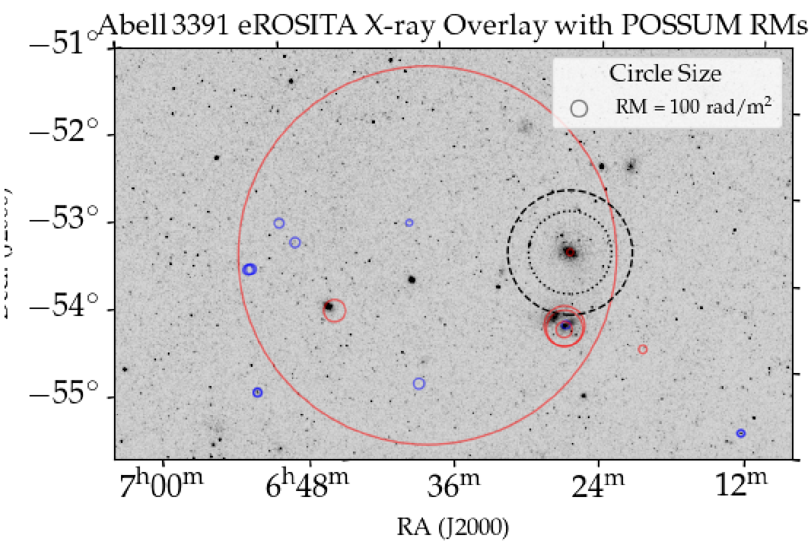

Figure 4.14: Image of the X-Ray data from eROSITA and the POSSUM RRMs overlaid on top for the Abell 3391 cluster.

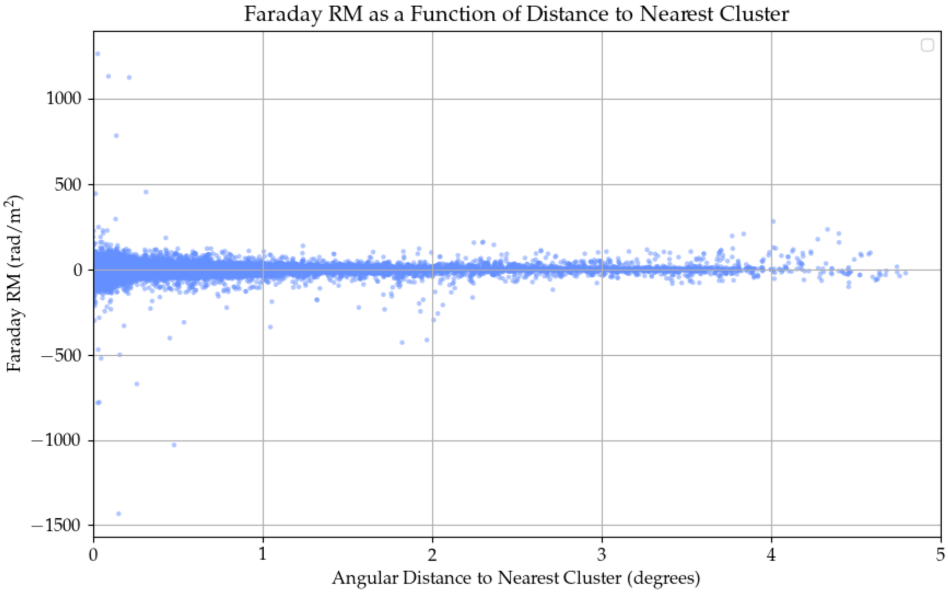

Figure 4.15: POSSUM Faraday RMs plotted as a function of distance to the nearest cluster. It is apparent that RM values increase when they are close to clusters up to about ≈ 0.5 degrees separation.

4.5 RM Enhancements Associated with the Broader Galaxy Cluster Population

I have included a second part of the analysis that seeks to determine whether the association of RM outliers with my small sample of individual galaxy clusters extends to the broader galaxy cluster population. This approach improves context and interpretation that cannot be achieved when looking at clusters in isolation. This portion of the analysis introduces a quality versus quantity dimension: in my original sample, I analysed several RM sightlines through a few clusters, while here, I seek to probe fewer sightlines but across a larger number of clusters. I cross-matched all POSSUM RMs to date with a comprehensive list from Wen and Han [2024] of 1.58 million galaxy clusters identified from the DESI Legacy Imaging Surveys, and I plotted the RM vs separation to these clusters. It is apparent that there is an excess of high RM sources closer to clusters, but it is crucial that I validate whether this effect is attributed to the clusters or not. Figures 4.15 and 4.16 show the angular distance to the nearest cluster vs RM at different ranges of angular distance to the nearest cluster or zooms. The most extreme outliers occur out to ≈ 0.5 degrees separation from the cluster centre. In Figure 4.17 I plot the physical scale vs. the redshift that it corresponds to. The conversions follow the same process as in Section 5.3. Note that this is much larger than the core radius of clusters.

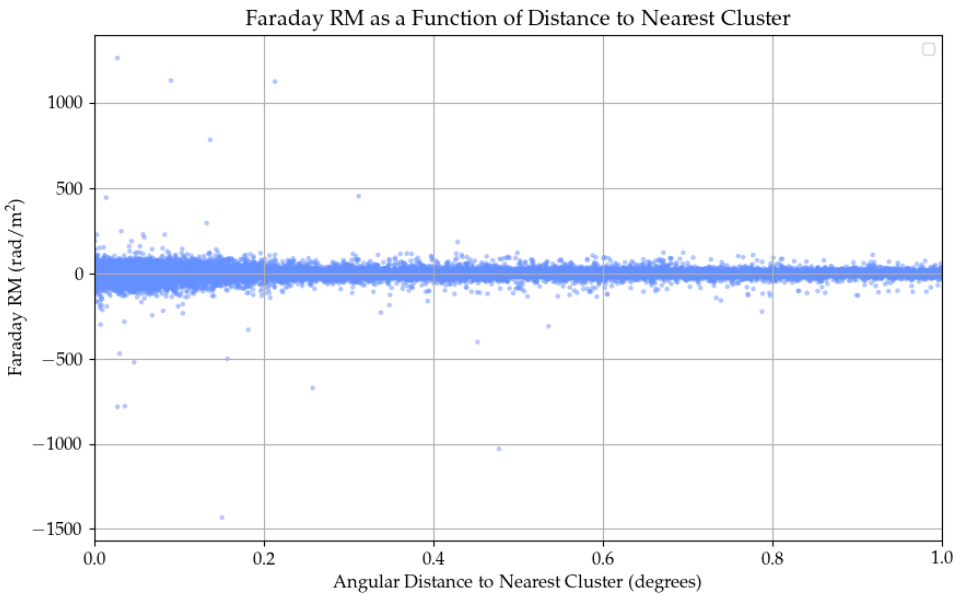

Figure 4.16: Similar to 4.15, but a more zoomed in look at RMs with a very small angular distance to the nearest cluster.

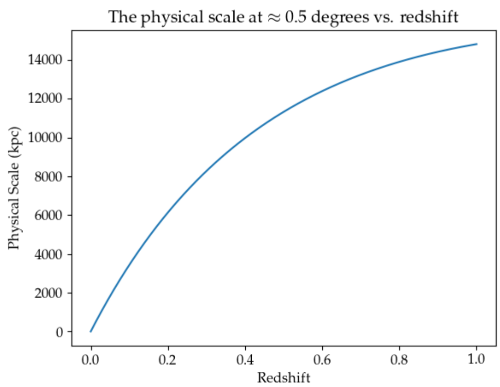

Figure 4.17: Physical Scale at ≈ 0.5 degrees separation vs. redshift that it corresponds to.

As in section 4.3 where K-S tests were conducted, these tests were also conducted between the two RM zooms. The result of the test tells us how likely they are from the same distribution of RMs. The first sample masked sources less than the angular scale characteristic of the virial radius for the cluster sample (0.6 degrees) and greater than the angular scale characteristic of the splashback radius for the cluster sample (1 degree). The other sample masked sources less than the angular scale characteristic of the splashback radius and greater than 5 degrees from the nearest cluster. The MAD of the characteristic infall region (RMs between the characteristic virial radius and characteristic splashback radius) is 9.15 rad/m/m, and the MAD beyond the characteristic splashback radius until 5 degrees from the cluster centre is 10.40 rad/m/m. We can see that the RM dispersion is increasing with distance from the cluster (between 0.6-5 degrees separation). From comparing these two samples, the resulting p-value was 1.10×10^{-14} and the k-s statistic was 0.0636. This p-value strongly supports the rejection of the null hypothesis which implies that there is asymmetry in the RRM dispersion of clusters and that the infall region and the region beyond the splashback radius have significantly different RRMs distributions.

Chapter 5

Discussion

The main results of this thesis that I will further discuss in this chapter include:

- Coherent features of elevated |RRMs| within and beyond the infall region of the Triangulum Australis cluster. A large RRM observed beyond the splashback radius, along with another significant RRM located near the splashback radius of the Abell 3391 cluster.
- Increasing RRM dispersion with radius in the Triangulum Australis cluster, and that quadrants containing the visually identified RRM features had higher measured RRM dispersion values.
- That for the first feature in the Triangulum Australis cluster, the probability of observing such a high areal density of outliers was 7.11×10^{-6}, and 5.61×10^{-87} for the second feature, when compared against the RRMs of the broader cluster. The difference in the RRM population of the visually identified features was also significant when compared to a null area at a similar latitude.
- The RRM outliers in the Triangulum Australis cluster in the infall region showed statistically significant clumping when using Ripley's K test.
- The p-values obtained from two-sample Kolmogorov-Smirnov (K-S) tests strongly support the rejection of the null hypothesis, which is where the two samples come from the same RRM distribution. This implies that there is asymmetry in the distribution of the RRMs of the Triangulum Australis cluster and the Abell 3391 cluster, and that the RRMs in the features in both clusters are significantly different to the RRMs in other areas of comparison.
- No evidence found for artefacts in Stokes I associated with the RRM enhancements in the Triangulum Australis cluster, and there was evidence for diffuse emission or potentially other cluster subcomponents associated with the features in the Triangulum Australis cluster.
- Asymmetry in the X-ray emission in the Triangulum Australis cluster which implies that the cluster is disturbed. There was also evidence of X-ray emission coincident with the RRM enhancements near the infall region of the Abell 3391 cluster.

- In the broader galaxy population there is asymmetry in the RRM dispersion of clusters and it implies that the infall region and region beyond the splashback radius have significantly different RRMs distributions.

5.1 Data Quality

I will note before I discuss interpretations of the analysis and results, that data quality as mentioned in Section 3.2, was shown to be an issue in the POSSUM data for at least one of the clusters in my sample. These issues manifested as alternating coherent patches of opposite signed RMs that were approximately the same size throughout the field. While visual inspection did not reveal the same issues in other fields, I cannot rule out that more subtle manifestations of this affect the results I discuss below. RM enhancements and subsequent interpretations are made with this caveat. Issues such as what I identified can manifest as false signals in cluster science since they appear as clusters of RMs, which is usually a sign of magnetised gas in galaxy clusters. To avoid this issue, I recommend that POSSUM researchers should look out in the data for patches of positive RMs, negative RMs, and patches of no RMs, as well as clustering of RRMs that appear in a pattern across the cluster or tile. I further recommend that future work could ameliorate this by only including galaxy clusters at a high Galactic $|b|$, which would mean that the Galactic foreground would be less of an issue. However, since diffuse ISM synchrotron emission does cover much of the sky, there is a diffuse subtraction pipeline in development. I have submitted my data as a testbed for these algorithms. The main results of this thesis involve solely the Triangulum Australis cluster, which shows different structure to the poor data quality in the Abell 3667 cluster. While a single detection like this is inherently limited, it is now supported by two other recent and as-yet unpublished POSSUM discoveries of large-scale coherent RRMs in other clusters not in my sample (Alonso+ in prep., Stuardi+ in prep), as well as the recent discovery of a filament of negative RMs cutting across the cluster Abell 3581 that would have been included in my sample based on the selection criteria in Section 3.3, but which was observed too late to conduct detailed analysis on (see Chapter 6). As such, for the remainder of this thesis I will proceed on the basis that the RM enhancements are associated with the cluster.

5.2 Physical Interpretation of RM Enhancements

In the Triangulum Cluster, there are features that could be consistent with magnetised gas falling into the cluster, or shocks in the infall region as shown in Figure 4.3. The angular size of the first feature was 2.9 degrees and had an RRM dispersion of 20.2 rad/m/m. The second feature had an angular size of 1.0 degrees and an RRM dispersion of 49.3 rad/m/m. Given the strength of the RRMs (≈ 100 rad/m/m) in these features being somewhat higher than the order of magnitude expected [Bonafede et al., 2013], the large angular spatial extent of the RRMs, and the correlations with the X-ray and Stokes I data, it points towards the features most likely being infalling streams of magnetised gas. In the Abell 3391 cluster, there is a large RRM value beyond the splashback radius and another substantial RRM value close to the splashback radius. Given the high strength of the RRMs in relative isolation of other RRMs of similar strength, it is possible that these RRMs are pointing out shocks outside the splashback radius of the cluster [Johnston-Hollitt et al., 2015]. The measured quadrant-based RRM dispersions of the Triangulum Australis cluster and the Abell 3391 cluster also show heightened MAD values in the quadrants corresponding to the RRM enhancements visually identified. The coherent RRM enhancements were also determined to be outliers with the number of clustered RRM outliers being statistically significant. When I was determining the likelihood of the RRM outliers being associated with the clusters versus the Galactic foreground contamination, it was crucial that I incorporate a null test (see Section 4.3.1. The challenge of determining whether RRM outliers are associated with the cluster itself is inherent in this type of study, however since the null area did not show any patterns or clustering in the distribution of RRM outliers, I conclude that it would be highly unlikely that most of the RRM outliers are associated with the Galactic foreground.

It has been predicted using simulations that there are asymmetric gas flows in the outer regions of clusters [Simionescu et al., 2021; Zhang et al., 2020]. The increasing RRM dispersion of the Triangulum Australis with increasing radius from the cluster centre as shown in 4.1, and the increasing RRM dispersion in the quadrants containing the features in the Triangulum Australis as shown in 4.2, could indicate that there is asymmetric gas flows near/in the infall region of the cluster. Asymmetrical gas flows are indicative of cosmic gas accretion and accretion shocks as mentioned in Section 2.6.

In section 4.3 I calculated the Ripley's K function to determine the scale-size of clustering of outlier RRM values for the Triangulum Australis cluster, the Abell 3391 cluster and the null region. Anderson et al. [2021] found fluctuations in the spatial density of RMs for the Fornax cluster. However, the cosmic variance of areal polarised source density remains poorly known, and it is unclear if polarised source density fluctuates across the sky, or whether it is an effect unique to clusters. There is also limited understanding of the clustering scales of extragalactic radio sources. Rudnick et al. [2007] also noted clustering of total intensity sources for uncertain reasons. The clustering of RMs seen near the infall region of the Triangulum Australis cluster are unlikely the result of galactic foreground or data quality issues given their spatial coincidence with the cluster, and the lack of evidence of such in our null test field at similar Galactic latitude. Instead I suggest that the clustering of RRMs are due to infalling magnetised gas. The clustering scale or value of K(r) in the infall region of the Triangulum Australis cluster is between 5-10 rad/m/m. For the null area, which is in an area covered by POSSUM, not overlapping any other clusters in my sample, and at a similar latitude to the Triangulum Australis cluster, the Ripley's K test shows little difference between the theoretical lines and the data, which means that there was little RRM clustering. Therefore, for gas filaments or shocks I would expect clustering on a scale greater than 1 rad/m/m.

As mentioned in Section 4.4, in the Stokes I map overlay plots in Figures 4.11 and 4.12, there was no evidence for artefacts associated with the RRM enhancements, but there was evidence for diffuse emission or possible cluster subcomponents in the infall region near the first feature and associated with the RRM enhancements in the second feature. Further in-depth X-ray analysis is needed to understand the nature of this emission. This would suggest that there is magnetised gas or shocks here. Shocks can also create relics and pheonixes (diffuse Stokes I emission) however these are relatively faint features ($\leq 1\mu$Jy/arcsec) [Gaensler et al., submitted]. As seen in the X-ray overlay plots in Figures 4.13 and 4.14, there appears to be some asymmetry in the X-ray emission associated with the core of the Triangulum Australis cluster, which implies that the cluster is disturbed. A disturbed cluster is usually associated with active accretion and dynamical shocks. While it is beyond the scope of this thesis, future work can exploit advanced X-ray mapping techniques such as Voronoi binning to search for faint X-ray counterparts to the RM signatures. This would provide a direct measure of thermal electron density, so that the RRMs can then be used to measure the embedded magnetic field strength directly.

5.2.1 Implications of This Work for the Prevalence of Detecting RM Enhancements at the Periphery of Galaxy Clusters

In this thesis, I have a sample of six clusters with two candidate detections, along with another apparent detection in a recently observed system which is mentioned in Chapter 6. I have also identified more subtle signals through statistical analysis. From $\approx 20\%$ of the POSSUM survey data analysed in this work, I appear to detect RRM enhancements in two clusters, suggesting that POSSUM will be able to analyse the extended gaseous envelopes of at least 10 clusters when complete. The additional three candidate detections by Stuardi+(in prep) and Alonso+(in prep), which use the same POSSUM data, as well as the more recently observed object in Chapter 6, suggests this number could be even higher. Furthermore, the upcoming Square Kilometre Array (SKA) will likely deliver even more detections of RM enhancements with more statistical certainty given it will have an all-sky RM grid at twice the density, or targeted observations of galaxy clusters at even higher densities.

5.3 Magnetic Field Strength

Currently, estimates of magnetic field strengths using RM grids in clusters have fractional uncertainties of hundreds of per cent [Johnson et al., 2020]. This is also the case when the thermal particle density is known [Anderson et al., 2024]. However, for the observed RM dispersions, it is possible to make an estimate of the range of magnetic field strengths required to produce these RM dispersions. Despite the large fractional uncertainties, these estimates are the only observational estimates of magnetic field strengths in these cosmic environments. Magnetic field strength scalings toward cluster peripheries appear to diverge significantly from theoretical models and simulations [Osinga et al., 2024]. This makes my estimates beyond cluster peripheries particularly important, as they provide crucial observational insights in a field where such data is scarce.

Following Gaensler et al. [2001] we have the relation:

$$\frac{\sigma_{RM}}{\mathrm{rad/m^2}} = \frac{812}{2\sqrt{3}} \left(\frac{n_e}{\mathrm{cm^{-3}}}\right) \left(\frac{B}{\mu G}\right) \sqrt{\left(\frac{L}{\mathrm{kpc}}\right)\left(\frac{l}{\mathrm{kpc}}\right)}$$

where σ_{RM} is the RM dispersion, n_e is the electron density, B is the magnetic field strength, L is the Intra-Cluster Medium (ICM) or magnetised gas path length, and l is the magnetic field correlation scale.
As discussed previously, the RM dispersion can be found by calculating the Median Absolute Deviation (MAD) of the foreground-corrected RM values in a given region. To correct for the $\approx$ 6 rad/m/m scatter that the magnetised environments of the RM sources themselves contribute on average [Schnitzeler, 2010; Taylor et al., 2024], I calculated the quadrature difference of the observed RM dispersion and the intrinsic source contribution before calculating the magnetic field strength from the RM contribution of the cluster gas. The magnetic field strength was calculated for the features found in the Triangulum Australis cluster that I have concluded are likely to be associated with the cluster. I performed the calculation by Monte Carlo analysis, randomly selecting the quantities n_e, l, and L from suitable ranges derived from simulations or other measurements as detailed below. The thermal electron density was selected from $[10^{-5}, 10^{-4}]\mathrm{cm}^{-3}$ using the estimates appropriate for cluster peripheries found in Anderson et al. [2024] which was taken from the literature [Eckert, D. et al., 2013; Nugent et al., 2020; Angelinelli, M. et al., 2022; Robson and Davé, 2022]. Similarly the magnetic field correlation scale l was selected from [1/100,1] times the splashback diameter L since this characteristic is poorly known, following Anderson et al. [2024]. The path length was obtained from the projected angular diameter of the RM enhancements given the redshift of the cluster, which I then assume is equal to the depth of the feature along the line of sight for the purpose of this calculation. The angular distance was estimated looking at roughly the length of the features. The angular distances of the features had an uncertainty of $\approx$0.5 degrees and so the path lengths had an uncertainty of $\approx$1847 kpc. l and n_e were randomly sampled 10^5 times and the magnetic field strength was obtained and the resulting distribution for the magnetic field strength is shown in Figure 5.1 for both features of interest.

I performed these calculations for the first feature of the Triangulum Australis cluster, and the mean and mode of the magnetic field strength is 38 nG and 18 nG respectively. For the second feature, the mean and mode of the magnetic field strength is 261 nG and 103 nG respectively. I also performed the same calculations for the radial regions (i.e. inside the virial radius, the infall region, and beyond the splashback radius) as defined in Section 4.2. The characteristic path lengths for each of these regions were taken to be the virial diameter for the virial region, the difference between the splashback radius and the virial radius for the infall region, and the difference between 4 degrees from the cluster centre and the splashback radius for the region beyond the splashback radius. The mean and mode of the magnetic field strength for within the virial radius is 73 nG and 31 nG respectively, the mean and mode for the infall region is 317 nG and 151 nG respectively, and the mean and mode for beyond the splashback radius is 36 nG and 13 nG respectively.

The values of the magnetic field strength were compared to what Carretti et al. [2022] found for cosmic web filaments in the Large-Scale Structure (LSS) far outside clusters, which was 32 ± 3 nG. The values for the first feature and beyond the splashback radius were found to be on the same order of magnitude. This seems reasonable as it is expected that magnetic fields are weaker in the sparse gas in cosmic web filaments well beyond clusters, compared to cluster interiors. If the RRM enhancements are indeed associated with pristine gas coming in from the outside of the cluster, then it is expected that the magnetisation would be broadly similar to that of cosmic web filaments. The second feature's values and the infall region's values of the magnetic field strength were approximately an order of magnitude greater, but this could be due to the feature and infall region being closer to the cluster centre, and therefore experiencing more gas compression resulting in denser filaments. These values are also on the same order of magnitude as those obtained by Anderson et al. [2024], where the mode and mean of the magnetic field strength distribution was 0.2 μG and 0.6 μG respectively. This was for a galaxy group-centric environment in a likely denser environment in the WHIM from accretion or outflows. The second feature also has a smaller assumed path length which would affect calculations.

It is interesting that the values of the magnetic field strength within the virial radius are lower than those in the infall region, however this is likely due to the possibility of many magnetic field reversals in the turbulent cluster centre. The reversal scale is poorly known. If small, this can reduce the measured RMs, which can lead to an underestimate of the magnetic field in these regions. This is a topic of active investigation by other POSSUM projects. Future work can focus on building up a better picture of the magnetic field strengths which will allow for detailed comparison to simulations. The estimate of the magnetic field strength in a cosmic web filament by Carretti et al. [2022] was in agreement with cosmological simulations where primordial magnetic fields were amplified by 'astrophysical source field seeding'. Carretti et al. [2022] state that there are however other scenarios depending on whether only primoridal fields or additional astrophysical source seeding are involved that result in different filament magnetic field strengths between a few nG to a few tens of nG with varying upper limits [Akahori and Ryu, 2010, 2011; Gheller et al., 2015; Vazza, F. et al., 2015; Vazza et al., 2017; O'Sullivan et al., 2020; Arámburo-García et al., 2021]. Therefore, it is possible that various cosmic web filaments, magnetised

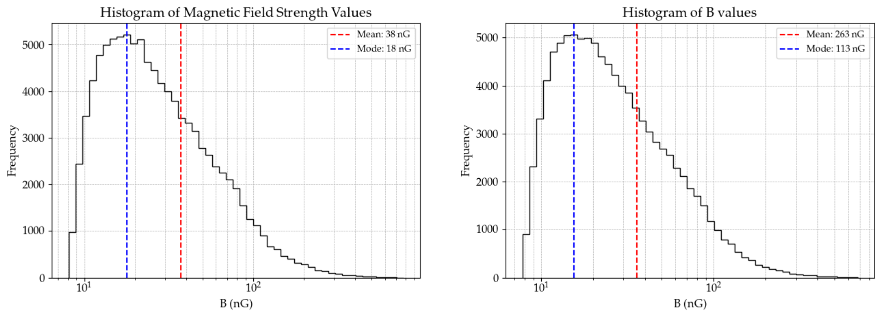

Figure 5.1: Histograms of the magnetic field strength values for both features of the Triangulum Australis cluster with log bins.

through different processes, are responsible for the observed variations in magnetic field strengths in the features in the Triangulum Australis cluster.

5.3.1 Orientation and Uniformity of the Magnetic Fields

The clear RRM enhancements seen in the Triangulum Australis cluster both consist of negative RRMs. This means that the magnetic fields are pointing away from us for these features as explained in Section 2.1. The uniformity of the magnetic fields is suggestive of a coherent feature, and points toward infalling magnetised gas as the likely cause since the magnetic fields are likely entrained in the gas flow, and so act as a kind of cosmic gas dye tracer. The significant RRMs seen in the Abell 3391 cluster are positive RRMs, which means that the magnetic fields are pointing towards us. I concluded that the extremely large RRM is likely associated with a shock.

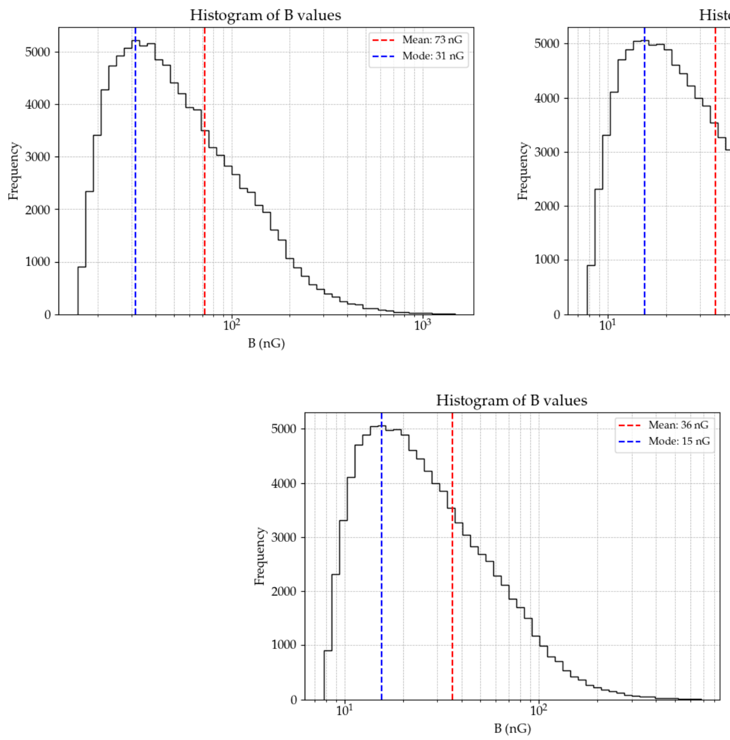

Figure 5.2: Histograms of the magnetic field strength values for the virial region (top left), the infall region (top right) and the region beyond the splashback radius (lower centre) for the Triangulum Australis cluster with log bins.

Chapter 6

Conclusions and Future Work

This thesis advances our understanding of the peripheral region of galaxy clusters using data from the Polarisation Sky Survey of the Universe's Magnetism (POSSUM). I analysed the outer regions of six galaxy clusters known to host hot gas with masses of at least 10^{14} solar masses and infall regions of at least 1 square degree. This represents the first ever systematic search for warm/hot magnetised gas in the peripheral regions of galaxy clusters, which is inaccessible to current X-ray and S-Z observations. My key findins are:

- I visually identified unusual coherent RRM variations, features, and RRM outliers (see section 4.3) in two out of the six clusters in my sample, which were qualitatively consistent with the expected signatures of magnetised, ionised gas at cluster peripheries. Two clusters in my sample exhibited notably unusual RM structures. The Triangulum Australis cluster showed an RM grid with a variety of structure, with one being a band of negative RRM values of width and length $\approx 1.5 \times 0.3$ degrees respectively, extending from the splashback radius outwards, and another being located at the splashback boundary to the north of the cluster. The Abell 3391 cluster showed an extraordinarily large RRM value of 1124 rad/m/m beyond the splashback radius, and another substantial RRM value close to the splashback radius.

- The RM enhancements I identified visually were verified through calculation of the spread of RRM values at different radii and azimuths.

- There are a large number of RRM outliers associated with cluster infall regions that are statistically significant. I evaluated the statistical significance of clustered RM outliers associated with cluster infall regions through a spatial randomness test. The resulting trends were complex, but more interestingly, showed a high clustering scale in the Triangulum Australis cluster and no clustering in the null area.

- I found evidence for either diffuse radio emission or cluster subcomponents in the infall region of the Triangulum Australis cluster using comparisons to total intensity radio emission. There were also no RRM enhancements associated with imaging artefacts.

- I found that the X-ray core was asymmetric in the Triangulum Australis cluster, which suggests a disturbed cluster undergoing active mergers or accretion.
- I determined how the association of RRM outliers with my cluster sample extends to the broader galaxy cluster population by way of a stacking experiment, which shows that there are outliers which extend until ≈ 0.5 degrees separation from the cluster centre. A future more sophisticated analysis would mask sources inside the virial radius of each cluster.
- I calculated the estimated magnetic field strengths for the coherent RM features of the Triangulum Australis cluster, as well as for the virial region, the infall region, and the region beyond the splashback radius for the Triangulum Australis cluster. The values of the magnetic field strength for one of the coherent RM features (mean and mode were 38nG and 18nG respectively) was on the same order of magnitude as expected for cosmic web filaments in the large-scale structure far outside clusters (32 ± 3nG). This implies that pristine gas is indeed coming in from the outside of the cluster.

Overall, the analysis conducted on my sample of six objects indicates that RM signatures of gas at the periphery of galaxy clusters are likely detectable in a notable subset of nearby clusters. This suggests that POSSUM and future RM surveys hold strong potential for identifying these features in a significant minority of observed systems. However, the scope of this project was designed so that all clusters meeting my selection criteria observed with POSSUM prior to October 2024 nominally constitute a part of my sample. Recently, the cluster Abell 3581, which met these criteria, was observed, processed, and deposited in CASDA. Visual inspection of the RM grid shows a prominent filament of negative RMs cutting across the cluster. Members of the POSSUM Collaboration have plotted a zoomed-out version that included the nearby clusters, and it appears to be a coherent cosmic RM filament, or bridge, between the clusters. Given that this discovery aligns with the goals and selection criteria (Section 3.3) of my project, and that such bridges are hypothesised to host a large fraction of the local universe's 'missing baryons' [Macquart et al., 2020], I will pursue this further. The POSSUM observations of this cluster, and subsequent discovery of the RM filament was in the later stages of my Honours, and therefore was not able to form part of the detailed analysis in this thesis. However, this discovery strengthens my thesis since a large, coherent RM structure linking clusters is similar to my findings of coherent RM patches near the periphery of clusters. The key difference being that the feature in the Triangulum Australis is limited to a region closer to the cluster centre, whereas the new structure spans across multiple clusters. Figure 6.1 shows the RM maps of the cluster Abell 3581 and surrounding clusters. Additionally Alonso et al (in prep), who have found a filament of gas linking clusters in the core of the Shapley supercluster via its RM signature, and Stuardi et al (in prep) who have discovered a filament connecting the clusters Abell 3365-51 using RM data. Combining this with my work, these findings suggest that RMs may provide one of the best observational tracers of a range of gas accretion phenomena at the peripheries

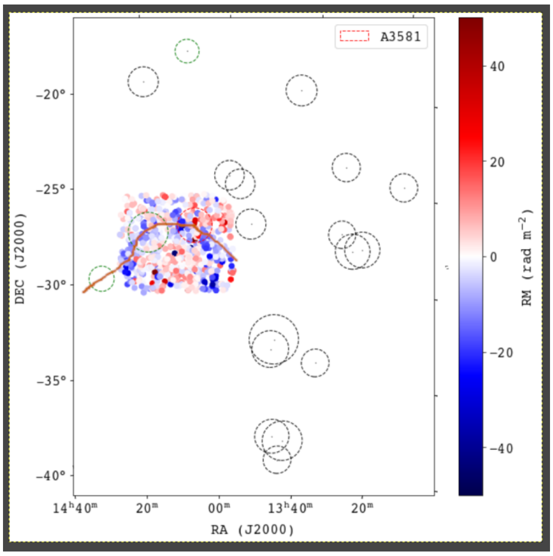

Figure 6.1: The RM grid of the Abell 3581 cluster which shows a prominent filament of negative RMs cutting across the cluster, highlighted with the orange line.

of galaxy clusters, which aligns directly with the goals of my project. As I mentioned previously in 5.2.1, I expect many more clusters to be observed by POSSUM to show the kind of RM enhancements I have discussed here. Since the POSSUM survey is $\approx$ 20% complete, and there have been at least 4 possible detections, I would expect at least 20 detections from galaxy clusters in the full POSSUM survey. As outlined in 1, the science goals of this thesis were to search for RM enhancements in six massive galaxy clusters in order to detect magnetised gas, shocks, and accretion flow outside the virial radii of clusters. With these larger sample sizes, future work could obtain the first reasonable observational view of gas accretion processes at cluster peripheries that could then be directly compared with cosmological simulations like Magneticum or IllustrisTNG. Future findings could also be combined with electron density tracers (such as fast radio burst dispersion measures or future, more sensitive X-ray and S-Z observatories) to directly infer magnetic field strengths and orientations.

This thesis has been limited by the RM data not being evenly distributed across the galaxy clusters, and not covering all scaled separations from each cluster. However, it should be kept in mind that the POSSUM survey is only $\approx$ 20% complete, and so the number of available RMs and sky coverage will increase considerably over the next few years. Future RM grid experiments will benefit from increased RM grid densities, and a more uniform and comprehensive coverage, which will enable more galaxy clusters to be examined for magnetised gas. The upcoming Square Kilometre Array (SKA), through more sensitive measurements, will also be able to provide denser RM grids.

Bibliography

Akahori, T. and Ryu, D., 2010. Faraday rotation measure due to the intergalactic magnetic field. *The Astrophysical Journal*, 723, 1 (oct 2010), 476. doi:10.1088/0004-637X/723/1/476. https://dx.doi.org/10.1088/0004-637X/723/1/476. (cited on page 48)

Akahori, T. and Ryu, D., 2011. Faraday rotation measure due to the intergalactic magnetic field. ii. the cosmological contribution. *The Astrophysical Journal*, 738, 2 (aug 2011), 134. doi:10.1088/0004-637X/738/2/134. https://dx.doi.org/10.1088/0004-637X/738/2/134. (cited on page 48)

Anderson, C. S.; Heald, G. H.; Eilek, J. A.; Lenc, E.; Gaensler, B. M.; Rudnick, L.; Van Eck, C. L.; OSullivan, S. P.; Stil, J. M.; Chippendale, A.; Riseley, C. J.; Carretti, E.; West, J.; Farnes, J.; Harvey-Smith, L.; McClure-Griffiths, N. M.; Bock, D. C. J.; Bunton, J. D.; Koribalski, B.; Tremblay, C. D.; Voronkov, M. A.; and Warhurst, K., 2021. Early science from possum: Shocks, turbulence, and a massive new reservoir of ionised gas in the fornax cluster. *Publications of the Astronomical Society of Australia*, 38 (Feb. 2021). doi:10.1017/pasa.2021.4. http://dx.doi.org/10.1017/pasa.2021.4. (cited on pages 2, 5, 7, 17, and 45)

Anderson, C. S.; McClure-Griffiths, N. M.; Rudnick, L.; Gaensler, B. M.; O'Sullivan, S. P.; Bradbury, S.; Akahori, T.; Baidoo, L.; Bruggen, M.; Carretti, E.; Duchesne, S.; Heald, G.; Jung, S. L.; Kaczmarek, J.; Leahy, D.; Loi, F.; Ma, Y. K.; Osinga, E.; Seta, A.; Stuardi, C.; Thomson, A. J. M.; Eck, C. V.; Vernstrom, T.; and West, J., 2024. Probing the magnetised gas distribution in galaxy groups and the cosmic web with possum faraday rotation measures. https://arxiv.org/abs/2407.20325. (cited on pages 15, 46, 47, 48, and 61)

Angelinelli, M.; Ettori, S.; Dolag, K.; Vazza, F.; and Ragagnin, A., 2022. Mapping out-of-the-box the properties of the baryons in massive halos. *A&A*, 663 (2022), L6. doi:10.1051/0004-6361/202244068. https://doi.org/10.1051/0004-6361/202244068. (cited on page 47)

Arámburo-García, A.; Bondarenko, K.; Boyarsky, A.; Nelson, D.; Pillepich, A.; and Sokolenko, A., 2021. Magnetization of the intergalactic medium in the IllustrisTNG simulations: the importance of extended, outflow-driven bubbles. *Monthly Notices of the Royal Astronomical Society*, 505, 4 (06 2021), 5038–5057. doi:10.1093/mnras/stab1632. https://doi.org/10.1093/mnras/stab1632. (cited on pages 17 and 48)

BECK, R. AND WIELEBINSKI, R., 2013. Magnetic fields in galaxies. *Planets, Stars and Stellar Systems*, 5 (2013), 641. doi:10.1007/978-94-007-5612-0_13. (cited on page 3)

BONAFEDE, A.; VAZZA, F.; BRUGGEN, M.; MURGIA, M.; GOVONI, F.; FERETTI, L.; GIOVANNINI, G.; AND OGREAN, G., 2013. Measurements and simulation of faraday rotation across the coma radio relic. *Monthly Notices of the Royal Astronomical Society*, 433, 4 (Jun. 2013), 32083226. doi:10.1093/mnras/stt960. http://dx.doi.org/10.1093/mnras/stt960. (cited on pages 20 and 44)

BULBUL, E.; LIU, A.; KLUGE, M.; ZHANG, X.; SANDERS, J. S.; BAHAR, Y. E.; GHIRARDINI, V.; ARTIS, E.; SEPPI, R.; GARREL, C.; RAMOS-CEJA, M. E.; COMPARAT, J.; BALZER, F.; BÖCKMANN, K.; BRÜGGEN, M.; CLERC, N.; DENNERL, K.; DOLAG, K.; FREYBERG, M.; GRANDIS, S.; GRUEN, D.; KLEINEBREIL, F.; KRIPPENDORF, S.; LAMER, G.; MERLONI, A.; MIGKAS, K.; NANDRA, K.; PACAUD, F.; PREDEHL, P.; REIPRICH, T. H.; SCHRABBACK, T.; VERONICA, A.; WELLER, J.; AND ZELMER, S., 2024. The srg/erosita all-sky survey: The first catalog of galaxy clusters and groups in the western galactic hemisphere. (cited on page 1)

CARRETTI, E.; OSULLIVAN, S. P.; VACCA, V.; VAZZA, F.; GHELLER, C.; VERNSTROM, T.; AND BONAFEDE, A., 2022. Magnetic field evolution in cosmic filaments with lofar data. *Monthly Notices of the Royal Astronomical Society*, 518, 2 (Oct. 2022), 22732286. doi:10.1093/mnras/stac2966. http://dx.doi.org/10.1093/mnras/stac2966. (cited on page 48)

CLARKE, T. E.; KRONBERG, P. P.; AND BÖHRINGER, H., 2001. A new radio-x-ray probe of galaxy cluster magnetic fields. *The Astrophysical Journal*, 547, 2 (jan 2001), L111. doi:10.1086/318896. https://dx.doi.org/10.1086/318896. (cited on pages 20 and 25)

ECKERT, D.; MOLENDI, S.; VAZZA, F.; ETTORI, S.; AND PALTANI, S., 2013. The x-ray/sz view of the virial region - i. thermodynamic properties. *A&A*, 551 (2013), A22. doi:10.1051/0004-6361/201220402. https://doi.org/10.1051/0004-6361/201220402. (cited on page 47)

GAENSLER, B.; HEALD, G.; MCCLURE-GRIFFITHS, N.; AND ANDERSON, C., submitted. The polarisation sky survey of the universe's magnetism (possum). i. science goals and survey description. (cited on pages xiii, 2, 4, 5, 7, 11, 28, 46, and 61)

GAENSLER, B. M.; DICKEY, J. M.; MCCLURE-GRIFFITHS, N. M.; GREEN, A. J.; WIERINGA, M. H.; AND HAYNES, R. F., 2001. Radio polarization from the inner galaxy at arcminute resolution. *The Astrophysical Journal*, 549, 2 (mar 2001), 959. doi:10.1086/319468. https://dx.doi.org/10.1086/319468. (cited on page 47)

GARDNER, F. AND WHITEOAK, J. J., 1966. The polarisation of cosmic radio waves. *Annual Review of Astronomy and Astrophysics*, 4 (1966), 245. doi:10.1146/annurev.aa.04.090166.001333. (cited on page 3)

GHELLER, C.; VAZZA, F.; FAVRE, J.; AND BRÜGGEN, M., 2015. Properties of cosmological filaments extracted from Eulerian simulations. *Monthly Notices of the*

Royal Astronomical Society, 453, 2 (08 2015), 1164–1185. doi:10.1093/mnras/stv1646. https://doi.org/10.1093/mnras/stv1646. (cited on page 48)

Hotan, A. W.; Bunton, J. D.; Chippendale, A. P.; Whiting, M.; Tuthill, J.; Moss, V. A.; McConnell, D.; Amy, S. W.; Huynh, M. T.; Allison, J. R.; Anderson, C. S.; Bannister, K. W.; Bastholm, E.; Beresford, R.; Bock, D. C.-J.; Bolton, R.; Chapman, J. M.; Chow, K.; Collier, J. D.; Cooray, F. R.; Cornwell, T. J.; Diamond, P. J.; Edwards, P. G.; Feain, I. J.; Franzen, T. M. O.; George, D.; Gupta, N.; Hampson, G. A.; Harvey-Smith, L.; Hayman, D. B.; Heywood, I.; Jacka, C.; Jackson, C. A.; Jackson, S.; Jeganathan, K.; Johnston, S.; Kesteven, M.; Kleiner, D.; Koribalski, B. S.; Lee-Waddell, K.; Lenc, E.; Lensson, E. S.; Mackay, S.; Mahony, E. K.; McClure-Griffiths, N. M.; McConigley, R.; Mirtschin, P.; Ng, A. K.; Norris, R. P.; Pearce, S. E.; Phillips, C.; Pilawa, M. A.; Raja, W.; Reynolds, J. E.; Roberts, P.; Roxby, D. N.; Sadler, E. M.; Shields, M.; Schinckel, A. E. T.; Serra, P.; Shaw, R. D.; Sweetnam, T.; Troup, E. R.; Tzioumis, A.; Voronkov, M. A.; and Westmeier, T., 2021. Australian square kilometre array pathfinder: I. system description. *Publications of the Astronomical Society of Australia*, 38 (2021). doi:10.1017/pasa.2021.1. http://dx.doi.org/10.1017/pasa.2021.1. (cited on page 5)

Ilani, G.; Hou, K.-C.; and Keshet, U., 2024. Excess cataloged x-ray and radio sources at galaxy-cluster virial shocks. (cited on page 9)

Johnson, A. R.; Rudnick, L.; Jones, T. W.; Mendygral, P. J.; and Dolag, K., 2020. Characterizing the uncertainty in cluster magnetic fields derived from rotation measures. *The Astrophysical Journal*, 888, 2 (jan 2020), 101. doi:10.3847/1538-4357/ab5d30. https://dx.doi.org/10.3847/1538-4357/ab5d30. (cited on page 46)

Johnston-Hollitt, M.; Govoni, F.; Beck, R.; Dehghan, S.; Pratley, L.; Akahori, T.; Heald, G.; Agudo, I.; Bonafede, A.; Carretti, E.; Clarke, T.; Colafrancesco, S.; EnSSlin, T.; Feretti, L.; Gaensler, B.; Haverkorn, M.; Mao, S. A.; Oppermann, N.; Rudnick, L.; Scaife, A.; Schnitzeler, D.; Stil, J.; Taylor, A. R.; and Vacca, V., 2015. Using ska rotation measures to reveal the mysteries of the magnetised universe. (cited on pages xiii, 3, 6, 7, 8, and 45)

Macquart, J.-P.; Prochaska, J. X.; McQuinn, M.; Bannister, K. W.; Bhandari, S.; Day, C. K.; Deller, A. T.; Ekers, R. D.; James, C. W.; Marnoch, L.; Osowski, S.; Phillips, C.; Ryder, S. D.; Scott, D. R.; Shannon, R. M.; and Tejos, N., 2020. A census of baryons in the universe from localized fast radio bursts. *Nature*, 581, 7809 (May 2020), 391395. doi:10.1038/s41586-020-2300-2. http://dx.doi.org/10.1038/s41586-020-2300-2. (cited on page 52)

Nugent, J. M.; Dai, X.; and Sun, M., 2020. Suzaku measurements of hot halo emission at outskirts for two poor galaxy groups: Ngc 3402 and ngc 5129. *The Astrophysical Journal*, 899, 2 (aug 2020), 160. doi:10.3847/1538-4357/aba691. https://dx.doi.org/10.3847/1538-4357/aba691. (cited on page 47)

Osinga, E.; van Weeren, R. J.; Rudnick, L.; Andrade-Santos, F.; Bonafede, A.; Clarke, T.; Duncan, K.; Giacintucci, S.; and Röttgering, H. J. A., 2024. Probing cluster magnetism with embedded and background radio sources in planck clusters. https://arxiv.org/abs/2408.07178. (cited on pages 25 and 47)

O'Sullivan, S. P.; Brüggen, M.; Vazza, F.; Carretti, E.; Locatelli, N. T.; Stuardi, C.; Vacca, V.; Vernstrom, T.; Heald, G.; Horellou, C.; Shimwell, T. W.; Hardcastle, M. J.; Tasse, C.; and Röttgering, H., 2020. New constraints on the magnetization of the cosmic web using LOFAR Faraday rotation observations. *Monthly Notices of the Royal Astronomical Society*, 495, 3 (05 2020), 2607–2619. doi:10.1093/mnras/staa1395. https://doi.org/10.1093/mnras/staa1395. (cited on page 48)

Ripley, B. D., 1976. The second-order analysis of stationary point processes. *Journal of Applied Probability*, 13, 2 (1976), 255266. doi:10.2307/3212829. (cited on page 30)

Robson, D. and Davé, R., 2022. Redshift evolution of galaxy group X-ray properties in the Simba simulations. *Monthly Notices of the Royal Astronomical Society*, 518, 4 (12 2022), 5826–5842. doi:10.1093/mnras/stac2982. https://doi.org/10.1093/mnras/stac2982. (cited on page 47)

Rudnick, L.; Brown, S.; and Williams, L. R., 2007. Extragalactic radio sources and the wmap cold spot. *The Astrophysical Journal*, 671, 1 (dec 2007), 40. doi:10.1086/522222. https://dx.doi.org/10.1086/522222. (cited on page 45)

Schnitzeler, D. H. F. M., 2010. The latitude dependence of the rotation measures of NVSS sources. *Monthly Notices of the Royal Astronomical Society: Letters*, 409, 1 (11 2010), L99–L103. doi:10.1111/j.1745-3933.2010.00957.x. https://doi.org/10.1111/j.1745-3933.2010.00957.x. (cited on pages 17, 25, and 47)

Simionescu, A.; Ettori, S.; Werner, N.; Nagai, D.; Vazza, F.; Akamatsu, H.; Pinto, C.; de Plaa, J.; Wijers, N.; Nelson, D.; Pointecouteau, E.; Pratt, G. W.; Spiga, D.; Vacanti, G.; Lau, E.; Rossetti, M.; Gastaldello, F.; Biffi, V.; Bulbul, E.; Collon, M. J.; Herder, J.-W. d.; Eckert, D.; Fraternali, F.; Mingo, B.; Pareschi, G.; Pezzulli, G.; Reiprich, T. H.; Schaye, J.; Walker, S. A.; and Werk, J., 2021. Voyage through the hidden physics of the cosmic web. *Experimental Astronomy*, 51, 3 (May 2021), 10431079. doi:10.1007/s10686-021-09720-0. http://dx.doi.org/10.1007/s10686-021-09720-0. (cited on pages 1, 6, 8, 9, 37, and 45)

Su, Y.; Kraft, R. P.; Nulsen, P. E. J.; Jones, C.; Maccarone, T. J.; Mernier, F.; Lovisari, L.; Sheardown, A.; Randall, S. W.; Roediger, E.; Fish, T. M.; Forman, W. R.; and Churazov, E., 2019. Extended x-ray study of m49: The frontier of the virgo cluster. *The Astronomical Journal*, 158, 1 (Jun. 2019), 6. doi:10.3847/1538-3881/ab1d51. http://dx.doi.org/10.3847/1538-3881/ab1d51. (cited on page 6)

Taylor, A. R.; Sekhar, S.; Heino, L.; Scaife, A. M. M.; Stil, J.; Bowles, M.; Jarvis, M.; Heywood, I.; and Collier, J. D., 2024. MIGHTEE polarization early science fields: the deep polarized sky. *Monthly Notices of the Royal Astronomical Society*, 528, 2 (01 2024), 2511–2522. doi:10.1093/mnras/stae169. https://doi.org/10.1093/mnras/stae169. (cited on pages 17, 25, and 47)

Taylor, A. R.; Stil, J. M.; and Sunstrum, C., 2009. A rotation measure image of the sky. *The Astrophysical Journal*, 702, 2 (aug 2009), 1230. doi:10.1088/0004-637X/702/2/1230. https://dx.doi.org/10.1088/0004-637X/702/2/1230. (cited on page 17)

Thomson, A. J. M.; McConnell, D.; Lenc, E.; Galvin, T. J.; Rudnick, L.; Heald, G.; Hale, C. L.; Duchesne, S. W.; Anderson, C. S.; Carretti, E.; Federrath, C.; Gaensler, B. M.; Harvey-Smith, L.; Haverkorn, M.; Hotan, A. W.; Ma, Y. K.; Murphy, T.; McClure-Griffith, N. M.; Moss, V. A.; O'Sullivan, S. P.; Raja, W.; Seta, A.; Eck, C. L. V.; West, J. L.; Whiting, M. T.; and Wieringa, M. H., 2023. The rapid askap continuum survey iii: Spectra and polarisation in cutouts of extragalactic sources (spice-racs) first data release. https://arxiv.org/abs/2307.07207. (cited on page 17)

Vanderwoude, S.; West, J. L.; Gaensler, B. M.; Rudnick, L.; Eck, C. L. V.; Thomson, A. J. M.; Andernach, H.; Anderson, C. S.; Carretti, E.; Heald, G. H.; Leahy, J. P.; McClure-Griffiths, N. M.; O'Sullivan, S. P.; Tahani, M.; and Willis, A. G., in press. Prototype faraday rotation measure catalogs from the polarisation sky survey of the universes 5 magnetism (possum) pilot observations. (in press). (cited on pages 2, 4, 6, and 28)

Vazza, F.; Brüggen, M.; Gheller, C.; Hackstein, S.; Wittor, D.; and Hinz, P. M., 2017. Simulations of extragalactic magnetic fields and of their observables. *Classical and Quantum Gravity*, 34, 23 (nov 2017), 234001. doi:10.1088/1361-6382/aa8e60. https://dx.doi.org/10.1088/1361-6382/aa8e60. (cited on page 48)

Vazza, F.; Ferrari, C.; Brüggen, M.; Bonafede, A.; Gheller, C.; and Wang, P., 2015. Forecasts for the detection of the magnetised cosmic web from cosmological simulations. *A&A*, 580 (2015), A119. doi:10.1051/0004-6361/201526228. https://doi.org/10.1051/0004-6361/201526228. (cited on page 48)

Wen, Z. L. and Han, J. L., 2024. A catalog of 1.58 million clusters of galaxies identified from the desi legacy imaging surveys. *The Astrophysical Journal Supplement Series*, 272, 2 (jun 2024), 39. doi:10.3847/1538-4365/ad409d. https://dx.doi.org/10.3847/1538-4365/ad409d. (cited on page 39)

Xu, W.; Ramos-Ceja, M. E.; Pacaud, F.; Reiprich, T. H.; and Erben, T., 2022. Catalog of x-ray-selected extended galaxy clusters from the rosat all-sky survey (rxgcc). *Astronomy and Astrophysics*, 658 (Feb. 2022), A59. doi:10.1051/0004-6361/202140908. http://dx.doi.org/10.1051/0004-6361/202140908. (cited on page 1)

Zhang, C.; Churazov, E.; Dolag, K.; Forman, W. R.; and Zhuravleva, I., 2020. Encounters of merger and accretion shocks in galaxy clusters and their effects on intracluster medium. *Monthly Notices of the Royal Astronomical Society*, 494, 3 (Apr. 2020), 45394547. doi:10.1093/mnras/staa1013. http://dx.doi.org/10.1093/mnras/staa1013. (cited on pages xiii, 8, 9, and 45)

Chapter 6

Appendix

6.1 POSSUM Data Processing Pipeline

If the objects in my sample had been processed with the POSSUM data processing pipeline or 1D pipeline, the data would have undergone this additional step after the observatory pipelines. It primarily performs convolution to survey resolution, correction for ionospheric Faraday rotation, tiling and reprojection, and mosaicking of overlapping/adjacent observations [Gaensler et al., submitted]. Unfortunately, only a small number of SBIDs were available at the time, so the data was obtained from CASDA, which, as mentioned before, is a data repository hosting POSSUM data. While this was not ideal, Anderson et al. [2024] has used this data successfully, and it is likely that only a small percentage of the data was affected by issues that the 1D pipeline would have fixed or flagged or removed.

6.2 Comparison of RM Features to Total Intensity Radio Emission

Shown below are the figures of the total intensity radio emission or Stokes I overlaid on the POSSUM RRMs for the other clusters in my sample that were not shown in Section 4.4.

6.3 Voronoi Figures

This section shows the Voronoi plots of the POSSUM RRMs for the other clusters in my sample not shown in Section 4.1.

6.4 Python Modules

Here is a list of all the python modules used in this work:

- Astropy
- Numpy

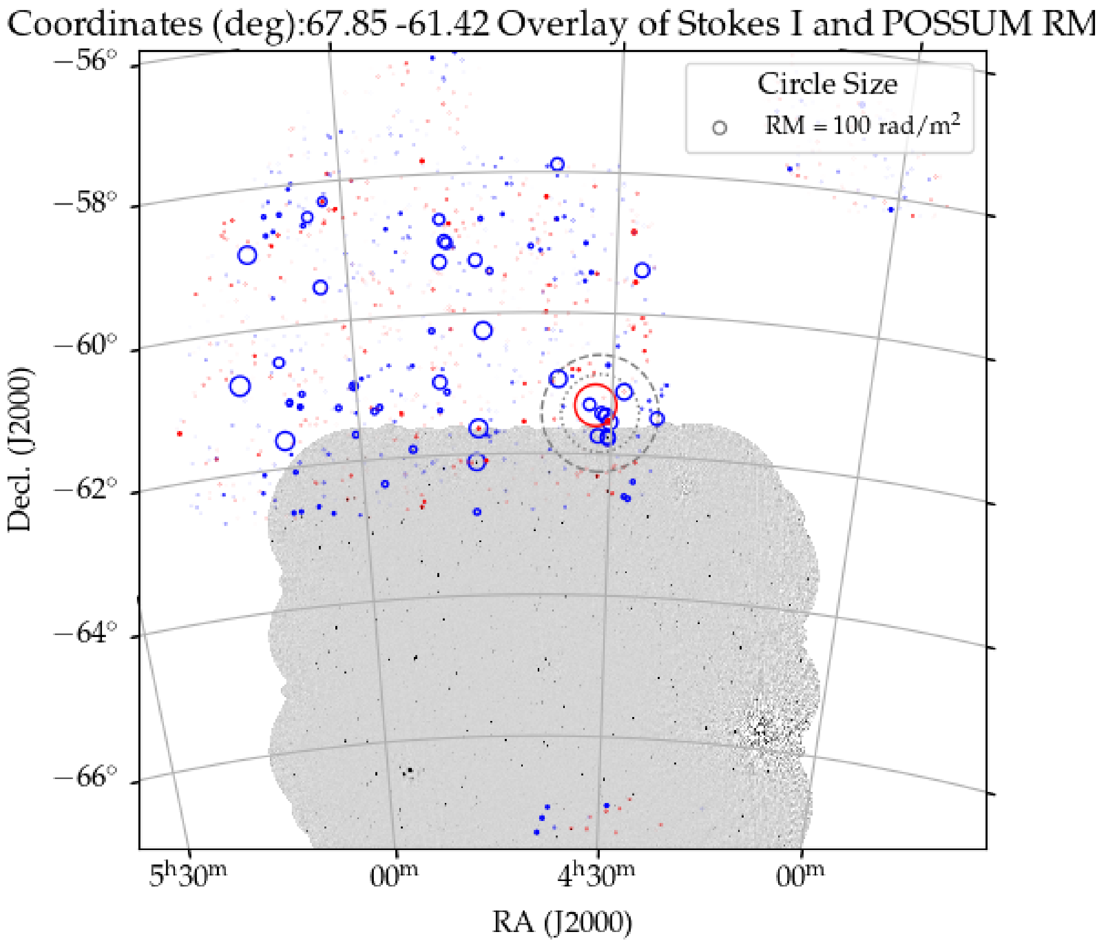

Figure 6.2: A figure of the Abell 3266 Cluster with the POSSUM RMs overlaid on the Stokes I map for that (grayscale) area. The dotted line is the virial radius and the dashed line is the splashback radius.

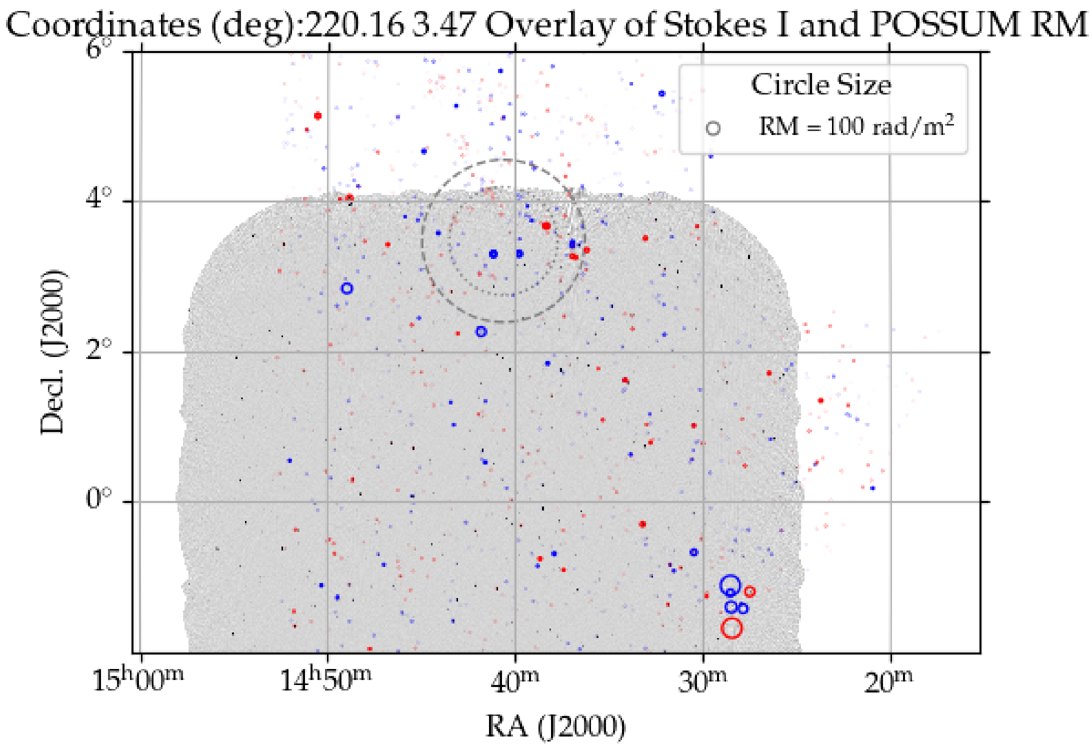

Figure 6.3: A figure of the MKW 8 Cluster with the POSSUM RMs overlaid on the Stokes I map for that (grayscale) area. The dotted line is the virial radius and the dashed line is the splashback radius.

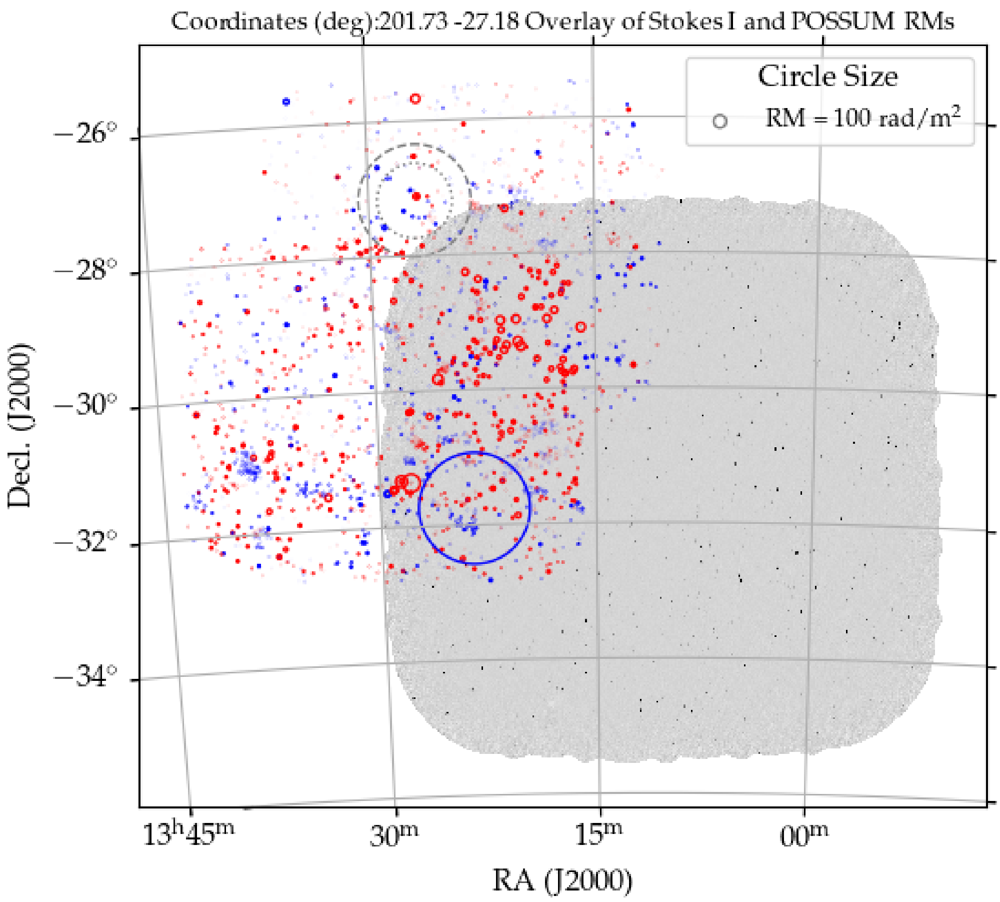

Figure 6.4: A figure of the Abell 1736 Cluster with the POSSUM RMs overlaid on the Stokes I map for that (grayscale) area. The dotted line is the virial radius and the dashed line is the splashback radius.

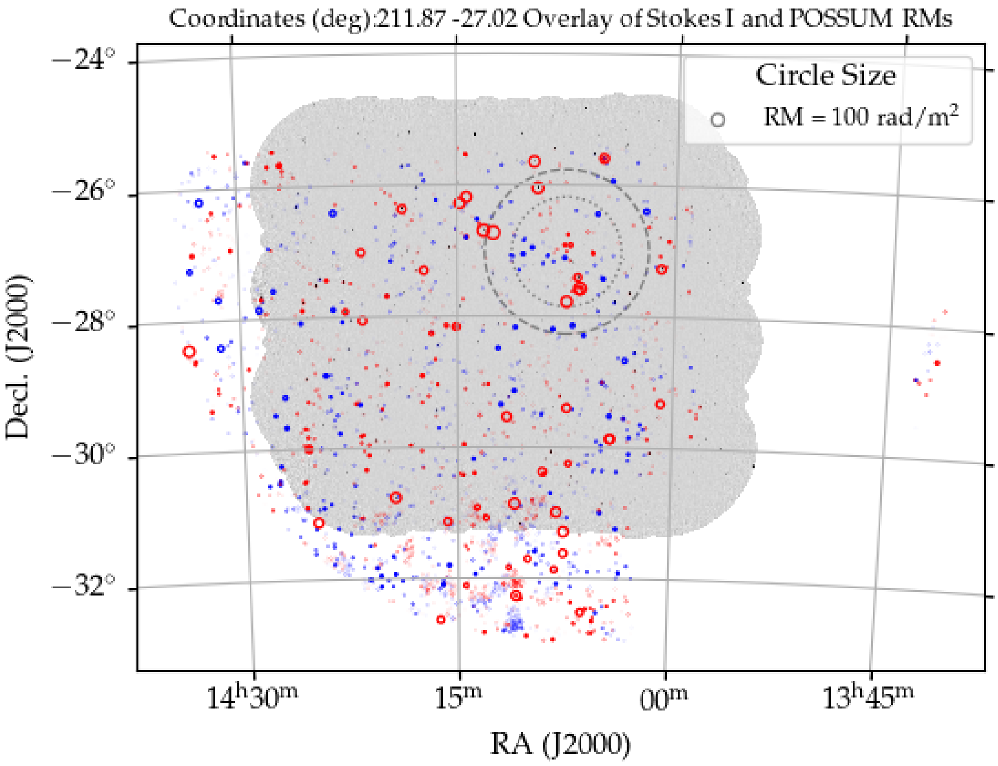

Figure 6.5: A figure of the Abell 3581 Cluster with the POSSUM RMs overlaid on the Stokes I map for that (grayscale) area. The dotted line is the virial radius and the dashed line is the splashback radius.

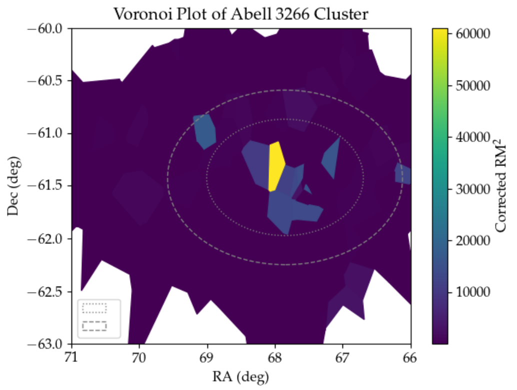

Figure 6.6: Image of the POSSUM Corrected RMs displayed in a Voronoi plot for the Abell 3266 cluster.

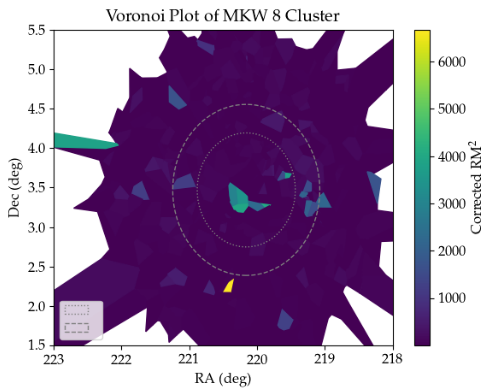

Figure 6.7: Image of the POSSUM Corrected RMs displayed in a Voronoi plot for the MKW 8 cluster.

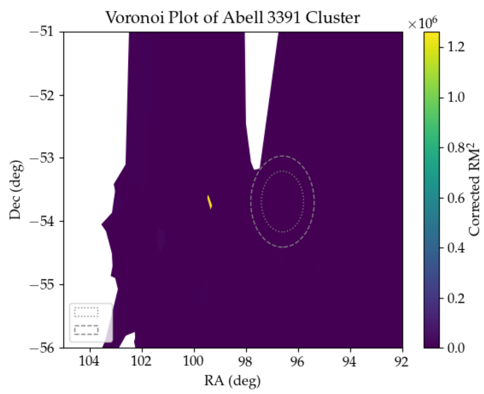

Figure 6.8: Image of the POSSUM Corrected RMs displayed in a Voronoi plot for the Abell 3391 cluster.

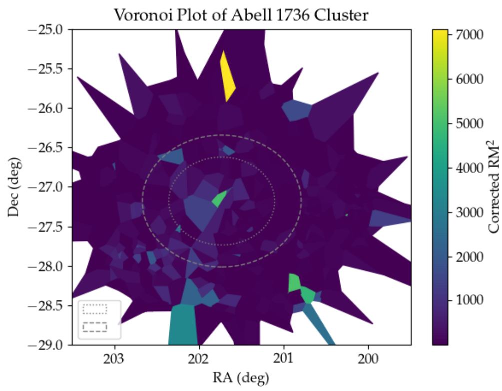

Figure 6.9: Image of the POSSUM Corrected RMs displayed in a Voronoi plot for the Abell 1736 cluster.

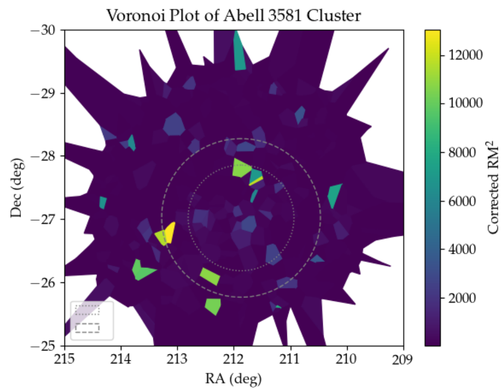

Figure 6.10: Image of the POSSUM Corrected RMs displayed in a Voronoi plot for the Abell 3581 cluster.

- Pylab
- Scipy
- Math
- Matplotlib
- PIL
- tarfile
- tqdm
- astroquery
- reproject
- pointpats

6.5 X-Ray Data Collection

To collect the eROSITA X-ray data, I used the software Aladin. I loaded the band 24 rate image, changed the pixel from preview to full dynamic and then cropped the region around the cluster. I convolved the image using the Gauss-4pix kernel. I then got the fits files of the X-ray images and overlaid them on the RRMs as done with the Stokes I overlays.